SPE 131732

Optimization of Multiple Transverse Hydraulic Fractures in Horizontal Wellbores

Bruce R. Meyer, SPE, Meyer & Associates, Inc.; Lucas W. Bazan, SPE, Bazan Consulting, Inc.; R. Henry Jacot, SPE, Atlas Energy Resources, LLC; and Michael G. Lattibeaudiere, SPE, Rosetta Resources, Inc.

This paper was prepared for presentation at the SPE Unconventional Gas Conference held in Pittsburgh, Pennsylvania, USA, 23-25 February 2010.

Abstract

Hydraulic fracturing and horizontal drilling are the two key technologies that have made the development of unconventional shale formations economical. Hydraulic fracturing has been the major and relatively inexpensive stimulation method used for enhanced oil and gas recovery in the petroleum industry since 1949. The multi-stage and multi-cluster per stage fracture treatments in horizontal wellbores create a large stimulated reservoir volume (SRV) that increases both production and estimated ultimate recovery (EUR).

This paper presents a new analytical solution methodology for predicting the behavior of multiple patterned transverse vertical hydraulic fractures intercepting horizontal wellbores. The numerical solution is applicable for finite-conductivity vertical fractures in rectangular shaped reservoirs. The mathematical formulation is based on the method of images with no flow boundaries for symmetrical patterns. An economics procedure is also presented for optimizing transverse fracture spacing and number of fracture stages/clusters to maximize the Net Present Value (NPV) and Discounted Return on Investment (DROI).

The advantages of this approximate analytical production solution for multiple finite-conductivity vertical transverse fractures in horizontal wells and corresponding optimization procedure include: 1) the solution is based on fundamental engineering principles, 2) the production and interference of multiple transverse fractures are predicted to a first-order, and 3) it provides the basis for optimizing fracture and cluster spacing based on NPV and DROI, not just initial production rate. The methodology provides a simple way to predict the production behavior (including interaction) and associated economics of multi-stage/multi-cluster transverse fracture spacing scenarios in horizontal wellbores.

The high initial production (IP) rates from multiple transverse fractures and the late time production decline as a result of fracture interference is discussed. Numerous examples are presented illustrating the method for optimizing (maximizing NPV and DROI) multiple transverse vertical hydraulic fractures in horizontal wellbores.

Application of this technique will help provide the design engineer with a better tool for designing and optimizing multi-stage/multi-cluster transverse hydraulic fractures in horizontal wellbores. The governing production equations and fundamental procedure for NPV and DROI optimization of transverse fractures in a horizontal wellbore are discussed.

Introduction

The large interest in developing unconventional shale reservoirs has been a direct result of the favorable economics achieved by the advancements in horizontal well drilling and hydraulic fracturing technologies. Since hydraulic fracturing is one of the most widely used and accepted methods for enhancing well performance, pressure transient analysis of fractured reservoirs has become an invaluable tool in determining the productivity and benefits of fracturing.

Hydraulic fracturing is the key technology for enhancing production in conventional and unconventional formations. The early work concentrated on solutions for infinite- and finite-conductivity vertical fractures intersecting vertical wells. Some of the early pioneers of this research are referenced below followed by contributors who have presented production solutions for multiple transverse fractures in horizontal wells.

McGuire and Sikora (1960) published a classic paper on “The Effect of Vertical Fractures on Well Productivity” demonstrating the productivity increase benefits from hydraulic fracturing as a function of fracture length (penetration) and relative fracture conductivity. Prats (1961) presented an analytical model for pseudosteady-state behavior of finite-

References and Appendices at end of paper.

conductivity vertical fractures. A wide variety of papers on pressure transient analysis of wells intersected by infinite, uniform flux, and finite-conductivity vertical fractures followed: e.g., Scott (1963), Russell and Truitt (1964), Raymond and Binder (1967), Tinsley *et al.* (1969), Ramey and Cobb (1971), Earlougher, Jr. *et al.* (1973, 1977), Gringarten, Ramey and Raghavan (1974), Raghavan and Hadinoto (1978), Gringarten (1978), Barker and Ramey (1978), Cinco-Ley *et al.* (1978, 1981, 1982), Lee and Brockenbrough (1983, 1986), etc.

Gringarten *et al.* (1974) studied the unsteady-state behavior of wells intersected by uniform-flux and infinite-conductivity fractures. Raghavan *et al.* (1978) also presented a mathematical model based on a constant-pressure outer boundary condition for uniform-flux and infinite-conductivity fractures. Cinco-Ley (1981, 1982) presented a new technique for performing pressure transient analysis for vertical finite-conductivity fractures using a bilinear flow model. Lee and Brockenbrough (1983) presented a landmark paper entitled "A New Analytical Solution for Finite Conductivity Vertical Fractures with Real Time and Laplace Space Parameter Estimation." This was the original analytical trilinear solution for finite-conductivity vertical fractures.

Soliman, Hunt, and El Rabaa (1988) published a paper on using analytical models to forecast production of multiple infinite-conductivity transverse fractures and to determine the optimum number of fractures in horizontal wells. Soliman illustrated that the optimum number of fractures depended on the formation and fluid properties. Yost and Overbey (1989) performed an analysis of multiple hydraulic fracturing treatments along a 2,000 foot horizontal wellbore in a naturally-fractured shale gas reservoir in West Virginia. The objective of their stimulation research in horizontal wellbores (among other studies) was to determine "the effects expected from hydraulically fracturing the well whenever multiple fractures would be induced."

Conlin *et al.* (1990) presented a paper on the numerical models built to determine the primary factors controlling the performance for Multiple Fracture Horizontal (MFH) wells drilled in the Dan Field located in the Danish North Sea. They concluded that "Numerical modelling can provide key insight into the factors governing MFH well behavior and can be used to improve future MFH well design."

Economidies *et al.* (1991), Larsen and Hegre (1991), and Raghavan *et al.* (1994) have all developed analytical solutions for horizontal wells with multiple hydraulic fractures. Economidies *et al.* developed a comprehensive numerical simulator to simulate diverse aspects associated with horizontal wells, including anisotropic medium with transverse and longitudinal hydraulic fractures of infinite- and finite-conductivity. Larsen presented general solutions for finite-conductivity vertical fractures intercepting horizontal wells and illustrated how data representing different flow regimes can be analyzed, especially for circular fractures. Raghavan *et al.* (1994) presented a mathematical model similar to that proposed by van Kruysdijk and Dullaet (1989) that discussed the three dominant flow regimes, provided boundary effects are negligible. The major regimes include: 1) an early-time flow-period where the system behaves as if the total flow rate is the flow rate for N commingled fractures, 2) an intermediate-time period that reflects the interference effects between fractures, and 3) a late-time period where the composite multiple transverse fracture system behaves as a single fracture with the length equal to the spacing between the outermost fractures.

Guo and Evans (1993), Larsen and Hegre (1994), and Horne and Temeng (1995) have presented analytical models for the inflow performance and transient behavior of a horizontal well with multiple transverse fractures. The mathematical model of Horne approximated the series of fractures as fully penetrating, uniform flux, vertical fractures in box-shaped closed reservoirs. The pressure transient solutions of these authors were first derived for a single vertical fracture of uniform flux using Green's and source functions as presented by Gringarten and Ramey (1973). The superposition principle was then applied to generate their final pressure transient solutions for multiple discrete fractures intersecting the horizontal well. Horne *et al.* also presented source functions for a closed-boundary system.

Elrafie and Wattenbarger (1997) investigated the viability of converting existing vertical wells into horizontal wells with multiple transverse fractures. Their numerical simulations used a gridded model with infinite-conductivity transverse fractures. Elrafie presented numerical simulation results for individual fracture rate performance in a multiple fracture system. Their results follow the conclusion of Raghavan (1994), that at early times, all rates are identical (for identical fracture properties) and at late times the central fractures produce at the lowest rates and the outermost fractures produce at the highest rates: "Basically, the inner fractures are shielded by the outer fractures." Elrafie presented a plot of normalized rate versus dimensionless time, which clearly illustrated that "the individual fractures rates are identical at early times, where at later times higher rates are seen from the outer most fractures." Elrafie also presented one of the first economic evaluations of multiple transverse vertical fractures in horizontal wells and concluded "Horizontal wells with multiple transverse fractures appear to make production of the Upper Bahariyia reservoirs economically feasible."

Kustamsi *et al.* (1997) evaluated and compared a number of multi-fractured horizontal well inflow models. The fracture inflow models consisted of both analytical and numerical models for infinite- and finite-conductivity fractures. The general presentation was focused on the various flow regimes and the mechanisms of fracture performance in horizontal wells. The

results of their study identified some of the best inflow models to be used under different scenarios. They concluded that "The inflow models provide reliable tools for predicting the well performance."

Medeiros *et al.* (2007) presented an analysis of production data for a hydraulically fractured horizontal well in a homogeneous reservoir using the transient productivity index. Solutions were presented for equally spaced transverse fractures in horizontal wells. Gilbert and Barree (2009) presented a paper on multiply production analysis in horizontal wells using an analytical model based on a single infinite-conductivity fracture solution package. Although the solution technique was not given, it was found to give accurate results for Multiply Fracture scenarios (i.e., for a constant flowing pressure, the total rate is a multiple of the single rate case).

Lolon *et al.* (2007) presented a paper on the application of 3-D numerical reservoir simulators for modeling transverse fractures in horizontal wells. Although 3-D reservoir simulators with finite-conductivity fractures (e.g., T.T. & Associates, Inc. (2009)) are used routinely today, grid refinement and inclusion of high conductivity elements to represent fractures may be very resource intense and time consuming. Automatic grid generators have certainly helped this process. The 3-D numerical results may also be dependent on the skills of the modeler. That aside, 3-D reservoir simulators are good tools for in-depth numerical analysis that cannot be handled satisfactorily with analytical first-order tools.

Brown *et al.* (2009) recently presented an analytical trilinear flow solution for multiply fractured horizontal well with equally spaced fractures using a symmetry element. They derived their solutions for "the outer reservoir, inner reservoir, and the hydraulic fracture and then coupled these solutions by using the flux and pressure continuity conditions on the interfaces between the regions." Numerous asymptotic approximations and flow regimes were presented with their trilinear model.

The enhanced production from multiple stage propped hydraulic fractures in horizontal wells is now making many of the unconventional tight shale plays, previously thought to be un-economical, the hot spots around the world. Although multi-stage/cluster transverse fracture treatments are very successful in stimulating these reservoirs, very little work has been done on multi-stage/cluster spacing optimization. The trend in the industry is for longer laterals with more stages/clusters with tighter spacing.

The purpose of this paper is to present a comprehensive methodology using the trilinear solution of Lee and Brockenbrough (1983, 1986) and the pseudosteady-state resistivity model of Meyer and Jacot (2005) for predicting the behavior (productivity) and economic optimization of multiple transverse finite-conductivity vertical fractures in horizontal wellbores. Numerous studies, limiting solutions, comparisons, and history matching with published data are presented. The methodology of transverse fracture optimization for a hypothetical gas shale is presented based on the economic concepts of NPV and DROI.

Mathematical Model

This section summarizes the governing equations describing the production solution for multiple transverse finite-conductivity vertical fractures in horizontal wellbores. Details of this methodology are given in the Appendices. The dimensionless parameters are summarized in Appendix A. Appendix B presents the trilinear solution of Lee and Brockenbrough (1983, 1986) and the pseudosteady-state resistivity model of Meyer and Jacot (2005). Appendix C presents the fundamental analytical production equations and solutions for a single fractured well in a closed system followed by general solutions for Multiply Fractures, Multiple Equally Spaced Transverse Fractures, and Multiple Stage/Cluster Transverse Fractures in horizontal wells. Appendix D provides a simple analytical solution for transverse fracture interference. The time for fracture interference is a function of the fracture spacing and formation diffusivity as formulated from the "Radius of Investigation Concept" by Lee *et al.* (1996, 2003). Appendix E presents the general economics equations for conducting net present value optimization. All symbols are defined in the Appendices and Nomenclature.

The numerical production solution is based on the following assumptions and boundary conditions:

1. The vertical transverse hydraulic fractures have a finite-conductivity (i.e., $0 \le C_{fD} < \infty$).
2. The formation is rectangular shaped with an aspect ratio of $\lambda = x_e / y_e$.
3. The formation is homogeneous.
4. The vertical fracture fully penetrates the formation (i.e., the fracture height is equal to the formation thickness).
5. The model accounts for restricted flow as a result of flow convergence at the wellbore in horizontal wells using a choked skin effect.
6. The model is derived for single phase oil and gas flow. Pseudo-pressure and time transformations are used for gas flow.

7. Formation fluid can only enter the wellbore through the fractures at the perforated intervals.
8. The pressure loss in the lateral (horizontal leg of the well) is negligible.
9. No flow outer boundaries are considered for closed reservoirs.
10. Multiple transverse fracture interaction is modeled using symmetry with no flow boundaries.
11. Darcy and non-Darcy flow in the fractures is considered.
12. The multiple transverse fractures are assumed to be identical (i.e., the same dimensionless conductivities and propped fracture characteristics).
13. The model does not account for desorption or changing fracture permeability as a result of a time dependent reservoir pressure.
14. The method of superposition is used for multi-rate and multi-pressure boundary conditions.

Trilinear Solution

The trilinear solutions of Lee and Brockenbrough (1983, 1986) for a finite-conductivity vertical fracture in Laplace space as presented in Appendix B for constant rate and pressure boundary conditions are

Constant Rate

$$p_D(s) = \frac{b}{s(sbC_{Df} - \psi \tanh \psi)} \tag{1}$$

Constant Pressure

$$q_D(s) = \frac{1}{s^2 p_D(s)} = -\frac{\psi}{sb} \tanh \psi \tag{2}$$

Pseudosteady-State Pressure Solution

The pseudosteady-state dimensionless pressure solution in a closed system can be written as (e.g., Ramey *et al.* (1971))

$$p_D = 2\pi t_{DA} + 1/J_D \tag{3}$$

where the inverse productivity index is given by

$$1/J_D = 1/2 \ln\left(\frac{4A}{e^{\gamma} C_A r_w'^2}\right) \tag{4}$$

Pseudosteady-State Resistivity Solution

The pseudosteady-state resistivity solution for a finite-conductivity fracture in a closed system in terms of the inverse productivity index as given by Meyer and Jacot (2005) is

$$\frac{1}{J_D} = \ln\left(\beta_{x_e} \frac{x_e}{x_f}\right) + f \tag{5}$$

where the pseudo-skin function, f, is

$$f = \ln\left(\frac{\pi}{C_{fD} g(\lambda)} + \zeta_{\infty}\right) \tag{6}$$

The above set of equations are solved to generate the production solution for a single fracture in a closed rectangular reservoir for all times (i.e., linear, bilinear, trilinear, and pseudosteady-state). These generated fundamental solutions for constant rate and constant pressure boundary conditions are then used to calculate the composite multiple transverse fracture solution as discussed below.

Wellbore Choked Skin Effect

Mukherjee and Economides (1991) identified that the inadequate contact between a vertical transverse fracture and the horizontal well resulted in a restriction that can be quantified by a choked skin effect as given by

$$S_{ch} = \frac{kh}{k_f w_f}\left[\ln\left(\frac{h}{2r_w}\right) - \frac{\pi}{2}\right] = \frac{h}{x_f}\frac{1}{C_{fD}}\left[\ln\left(\frac{h}{2r_w}\right) - \frac{\pi}{2}\right] \tag{7}$$

where the above equation has been placed in terms of the dimensionless fracture conductivity.

Eq. 7 illustrates that as the height interval to wellbore radius ratio or height to propped length ratio decreases (i.e., radial to linear flow in the fracture) or the dimensionless fracture conductivity increases, the skin due to convergence becomes smaller. Soliman *et al.* (1988) concluded that a high conductivity tail-in could be incorporated to reduce the additional pressure drop because of flow convergence around the wellbore.

Multiple Transverse Fracture Solution

Schematics for a number of general multiple transverse fracture patterns formulated in this paper are presented in Appendix C (e.g., see Figure 31 through Figure 34). The fundamental dimensionless pressure and rate solutions for multiple stage/cluster transverse fractures in horizontal wells as given in Appendix C are

Constant Rate

$$p_D = \frac{p_D(t_D, \lambda_c) \cdot p_D(t_D, \lambda_i) \cdot p_D(t_D, \lambda_e)}{p_D(t_D, \lambda_i) \cdot p_D(t_D, \lambda_e)(n_c - 1)n_s + p_D(t_D, \lambda_c) \cdot p_D(t_D, \lambda_e)(n_s - 1) + p_D(t_D, \lambda_c) \cdot p_D(t_D, \lambda_i)} \tag{8}$$

Constant Pressure

$$q_D = q_D(t_D, \lambda_c)(n_c - 1)n_s + q_D(t_D, \lambda_i)(n_s - 1) + q_D(t_D, \lambda_e) \tag{9}$$

These are not exact solutions, however, they are very good first-order approximations to a number of typical stage/cluster configurations. If the inner and cluster aspect ratios are equal (i.e., $\lambda_i = \lambda_c$), the constant rate and pressure solutions simplify to Eq. C.6 and Eq. C.7. For equally spaced fractures (i.e., $\lambda_e = \lambda_i = \lambda_c$), the above equations simplify to the Multiply Fractures solution (which is an exact solution) as given in Appendix C (i.e., Eq. C.3 and Eq. C.4)

Constant Rate

$$p_D = p_D(t_D, \lambda_c)/N \tag{10}$$

Constant Pressure

$$q_D = q_D(t_D, \lambda_c) \cdot N \tag{11}$$

where $N = n_c n_s$.

Transverse Fracture Rate Performance and Interaction

Elrafie and Wattenbarger (1997) presented numerical simulations for individual fracture rate performance in a multiple fracture system. As discussed above, their results followed the conclusion of Raghavan (1994), that at early times all rates are identical (for identical fracture properties) and at late times, the central fractures produce at the lowest rates and the outermost fractures produce at the highest rates. Elrafie presented a plot of normalized rate versus dimensionless time which clearly illustrated "individual fracture rates are identical at early times, where at later times higher rates are seen from the outer most fractures." The reservoir and fracture properties for this gas study are shown in Table 1.

Table 1. Interference Study - Reservoir and Fracture Properties.

Formation	Gas
Net Pay Thickness (ft)	50
Permeability (mD)	0.0005
HC Porosity (%)	5
Pore Pressure (psi)	3,400
Reservoir Viscosity (cp)	0.0176
Reservoir Compressibility (1/psi)	2.94e-04
Diffusivity (mD-psi/cp)	1932
Temperature ($^\circ F$)	260
Drainage Area (acres)	2300
Flowing BHP (psi)	500

Fracture/Wellbore	
Propped Length (ft)	1,500
Conductivity, $k_f w_f$, (mD-ft)	17.6
Dim. Conductivity, C_{fD}	15
Number Transverse Fracs	8
Lateral Length (ft)	2,000

Figure 1 shows the gas flow rate versus time for a well with eight transverse fractures equally spaced over a 2,000 foot lateral in essentially an infinite reservoir. As illustrated, the interior and exterior gas flow rates are identical until the time

of interference that occurs in approximately one year.

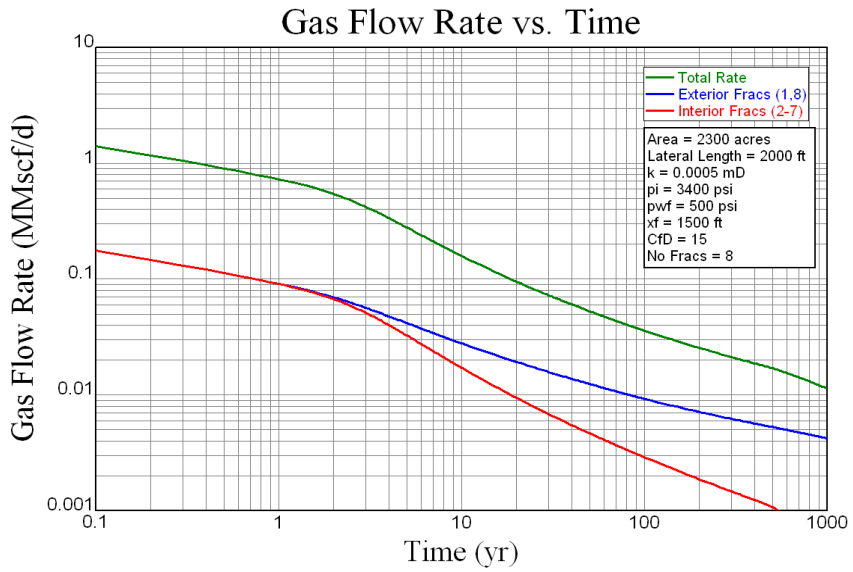

Fig. 1 — Interference: Total, interior, and exterior fracture gas flow rates versus time for eight multiple transverse fractures.

Figure 2 shows the interior and exterior normalized fracture rate performance for the multiple transverse fractures. As illustrated, the individual fracture rates are identical at early times and at later times the exterior or outermost fractures produce at the higher rates. Figure 3 shows the interior and exterior normalized fracture rate performance for the multiple transverse fractures in a linear zoom mode to highlight the time of fracture interference. The time of interference is shown to be about one year. The approximate time of interference from the data given in Table 1 using Eq. D.3 is $t = 237\Delta y^2/\eta$ = 10,000 hrs. (1.14 years).

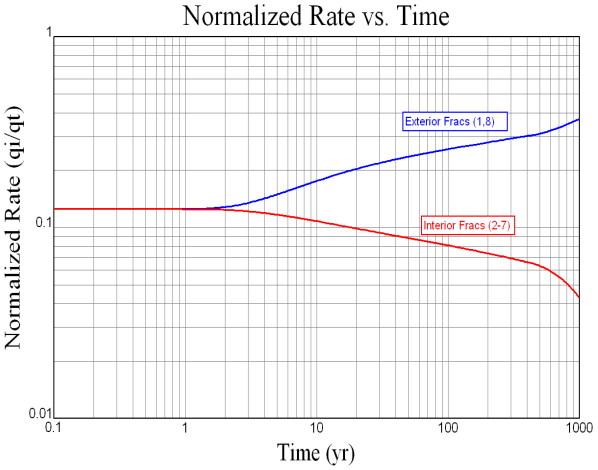

Fig. 2 — Normalized interior and exterior fracture gas flow rates versus time for eight multiple transverse fractures.

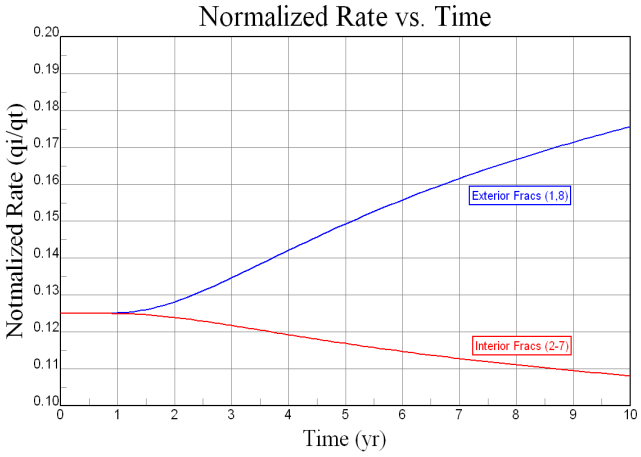

Fig. 3 — Normalized interior and exterior fracture gas flow rates versus time - ten years.

Cotton Valley Comparison

Lolon, Shaoul, and Mayerhofer (2007) performed a 3-D numerical simulation of multiple transverse fractures intersecting a horizontal well in the Cotton Valley formation. The objective of their study was to determine the optimum completion strategy of lateral length and number of fracture (transverse) stages. Although no economic analysis was performed, their analysis presented results for the effect of longer laterals and various numbers of multiple transverse fractures. A comparison of this analytical simulator with the 3-D numerical simulator of Lolon was made based on one to seven (1-7) equally spaced multiple transverse fractures over a 2,000 foot lateral in a 230 acre drainage area (note: Lolon *et al.* modeled 3-7 fractures). The Cotton Valley reservoir and fracture properties are shown in Table 2.

Table 2. Cotton Valley - Reservoir and Fracture Properties.

Formation	Cotton Valley
Depth (ft)	9,000
Net Pay Thickness (ft)	100
Permeability (mD)	0.001
Water Saturation (%)	50
Porosity (%)	7
Diffusivity (mD-psi/cp)	6857
Pore Pressure (psi)	6,000
Temperature ($^\circ F$)	285
Drainage Area (acres)	230
Flowing BHP (psi)	1,500

Fracture/Wellbore	
Propped Length (ft)	1,500
Conductivity, $k_f w_f$, (mD-ft)	114
Dim. Conductivity, C_{fD}	76
Number Transverse Fracs	1-7
Lateral Length (ft)	2,000

Since the 3-D simulation assumed a line source at the well, the choked skin effect as a result of convergence is not considered. However, even if choked skin was considered, it would be negligible ($S_{ch} = 0.003$).

Figure 4 presents the numerical results for the gas flow rate as a function of the number of transverse fractures versus time. As illustrated, because of interference as the number of transverse fractures increases, the total flow rate declines faster with time. Figure 4 also shows that at about 1,825 days of production, the flow rate from four or more multiple transverse fractures is about the same as from three fractures.

The cumulative gas production as a function of the number of transverse fractures with time is shown in Figure 5. A comparison of our analytical solution with the 3-D numerical results of Lolon illustrates very good agreement (i.e., demonstrating the multiple fracture solution methodology and pseudo-pressure/time formulation for gas flow). Figure 5 also illustrates that after 1,825 days of production the cumulative production from seven transverse fractures is only about 4.5 times that of a single transverse fracture.

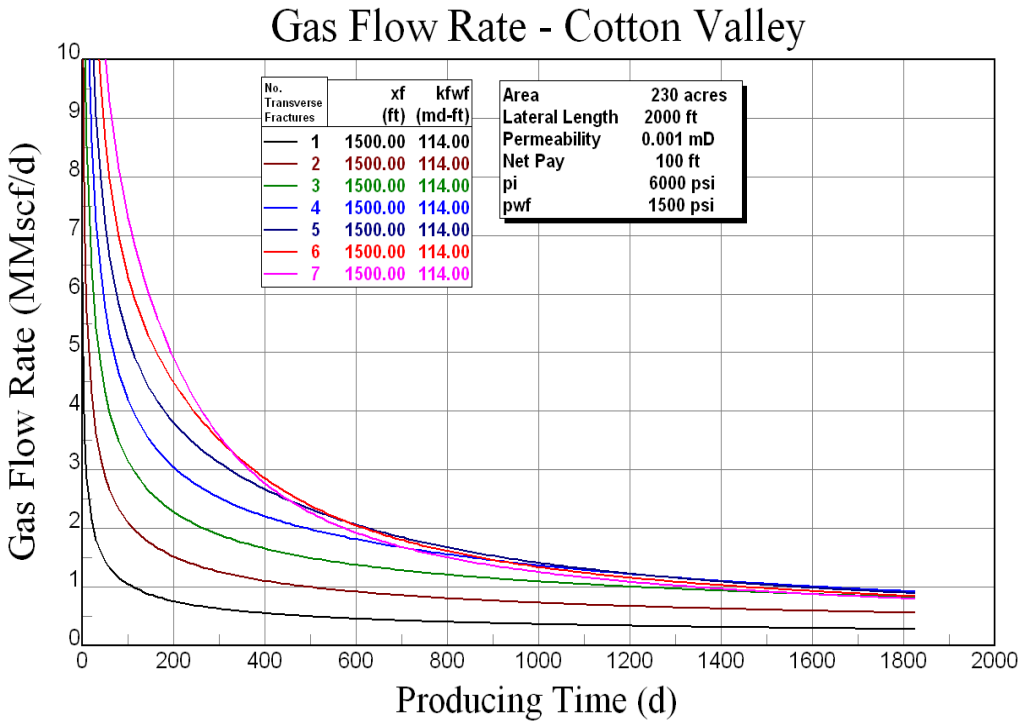

Fig. 4 — Cotton Valley - Gas flow rate versus time for multiple transverse fractures.

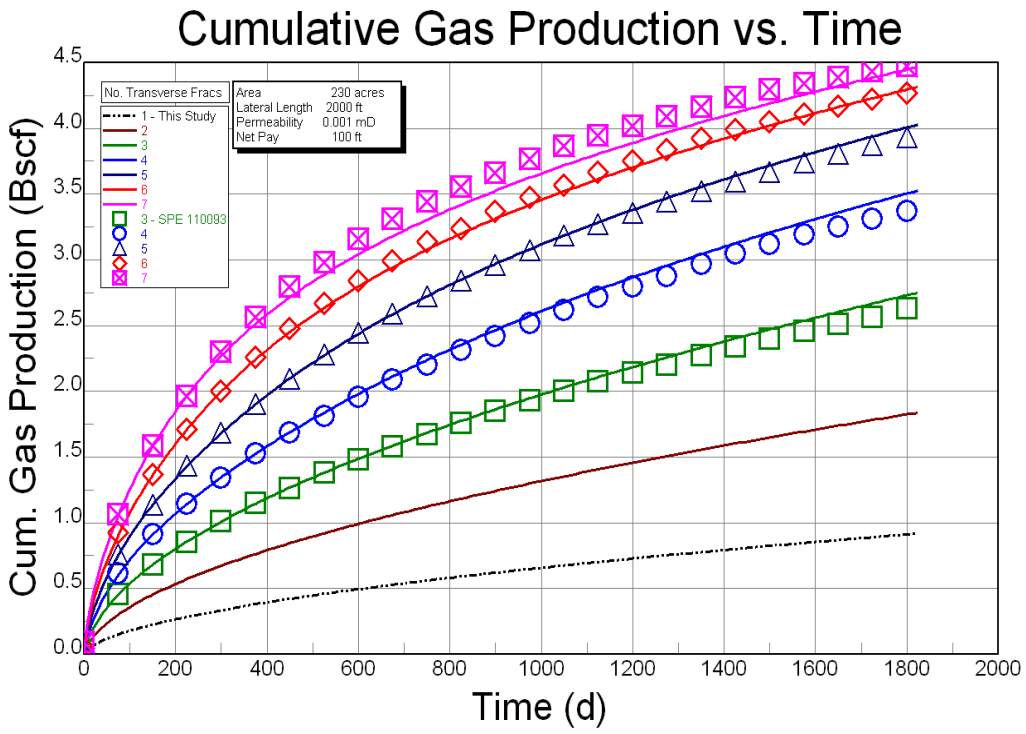

Fig. 5 — Cotton Valley - Cumulative production versus time for multiple transverse fractures.

Bakken Comparison

Lolon *et al.* (2009) performed a 3-D numerical simulation of multiple transverse fractures intersecting a horizontal well in the Bakken formation in North Dakota. The objective of their study was to perform a parametric reservoir simulation study to evaluate the down-spacing potential of horizontal wells in the middle Bakken formation. A comparison was made based on 1, 4, 6, 8, 10, and 12 equally spaced multiple transverse fractures over a 5,000 foot lateral in a 640 acre drainage area. The reservoir and fracture properties for the Bakken are shown in Table 3.

Table 3. Bakken - Reservoir and Fracture Properties.

Formation	Bakken
Depth (ft)	9,881
Net Pay Thickness (ft)	46
Permeability (mD)	0.002
Water Saturation (%)	0
Porosity (%)	5
Pore Pressure (psi)	4,900
Temperature ($^\circ F$)	209
Reservoir Compressibility (1/psi)	2.0e-05
Reservoir Viscosity (cp)	0.30
Diffusivity (mD-psi/cp)	6667
Drainage Area (acres)	640
Flowing BHP (psi)	1,500

Fracture/Wellbore	
Propped Length (ft)	420
Conductivity, $k_f w_f$, (mD-ft))	200
Dim. Conductivity, C_{fD}	238
Number Transverse Fracs	4, 6, 8, 10, 12
Lateral Length (ft)	5,000

Since the 3-D simulation assumed a line source at the well, the choked skin effect as a result of convergence is not considered. However, if the choked skin was considered it would be negligible ($S_{ch} = 0.00034$).

Figure 6 presents the numerical results for the oil flow rate as a function of the number of transverse fractures versus time. As illustrated, because of interference, as the number of transverse fractures increases the total oil flow rate declines at a steeper rate with time. After five years of production, the instantaneous flow rate from 10 transverse fractures is greater than the flow rate from 12 fractures.

The cumulative oil production as a function of the number of transverse fractures and time is shown in Figure 7. A comparison of our analytical simulation solution with their 3-D numerical results (quantified in an internal Oasis Petroleum report (2008)) illustrates the excellent agreement. Figure 7 also shows that after 5 years of production the cumulative production from 12 transverse fractures is only about 10 times greater than that of a single transverse fracture. The approximate time of interference for 10 transverse fractures from Eq. D.3 is $t = 237\Delta y^2/\eta = 10{,}970$ hrs. (457 days).

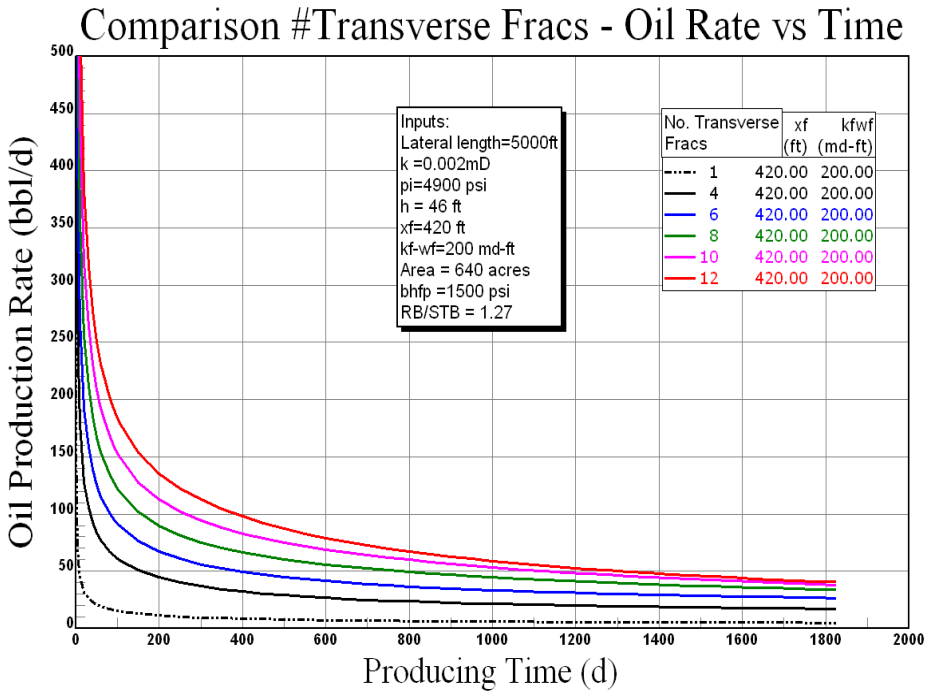

Fig. 6 — Bakken - Oil flow rate versus time for multiple transverse fractures.

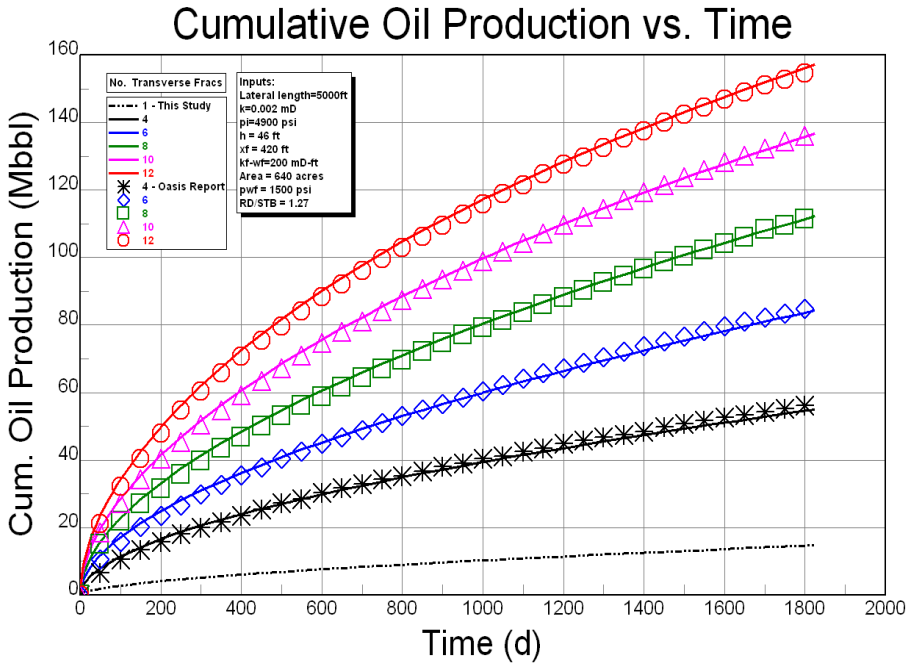

Fig. 7 — Bakken - Cumulative oil production versus time for multiple transverse fractures.

Marcellus Shale - History Match

The Marcellus shale is arguably the largest shale gas play in the lower 48 states. The Marcellus covers approximately

54,000 square miles, which extends through Pennsylvania, New York, Ohio, Maryland, and West Virginia. A new survey issued by Terry Englander, a geo-science professor at Pennsylvania State University, and Gary Lash, a geology professor at the State University of New York at Fredonia, surprised everyone when their research concluded that the Marcellus Natural Gas Shale Field could hold up to 500 trillion cubic feet of natural gas (Englander and Lash (2009)).

The Marcellus shale horizontal well was completed with a seven stage fracture treatment (five perforation clusters per stage) over a lateral of 2,100 feet. The treatment design for each stage consisted of 450,000 gallons slickwater and 400,000 lbm of sand which included 300,000 lbm of 100 mesh and 100,000 lbm of 40/70 resin coated sand. The treatment was originally designed for 100 bpm though the average treating rate was about 80 bpm because of higher than expected surface treating pressures.

Following the seven stage treatment, the well was flowed back and the plugs were drilled out with coil. After the well was cleaned out with coil tubing, a production log was run to determine flow contribution from each stage. The results of the production log showed a total gas flow rate of 3.166 MMscf/d and a water rate of 2,541 bpd. Stage two showed a minimal contribution of about 3% of the total production. Most stages also showed production from a single dominant cluster fracture. Therefore, only six multiple transverse fractures were used to history match the production data.

The production data was history matched with the single phase analytical reservoir simulator for multiple transverse finite-conductivity vertical fractures in horizontal wellbores as discussed above and in Appendix D. The effect of choked skin was also considered.

The Marcellus shale reservoir and history match results for the seven stage, five cluster/stage transverse hydraulic fracture treatment in a horizontal well are given in Table 4. The Marcellus shale history matched parameters are given in Table 5.

Table 4. Marcellus Shale - Reservoir and Fracture Properties.

Formation	**Marcellus**
Depth (ft)	7,876
Thickness (ft)	162
HC Porosity (%)	4.2
Pore Pressure (psi)	4726
Specific Gravity	0.58
Temperature ($^\circ F$)	175
Drainage Area (acres)	80
Aspect Ratio, $\lambda = x_e/y_e$	1/4
Reservoir Size (x_e, y_e), (ft)	(933.38, 3733.52)
BHFP (psi)	1450-530

Wellbore/Fracture	
Wellbore Radius (ft)	0.3646
Lateral Length (ft)	2,100
Number of Stages	7
Clusters/Stage	5

Table 5. Marcellus Shale - History Matched Parameters

Formation - Marcellus	**No Tail-in**	**Tail-in**
Permeability, k, (nD)	583	478
Reservoir Capacity, kh, (mD-ft)	0.094	0.077
Diffusivity, η, (mD-psi/cp)	4000	3300
Fracture		
Propped Length (ft)	320	363
Conductivity, $k_f w_f$, (mD-ft))	3.77	2.82
Dim. Conductivity, C_{fD}	20.2	16.3
Choked Skin, [1] S_{ch}	0.096	0.067[3]
Number Equivalent Fracs[2]	6	6
Error (%)	1.3	1.3
Std. Dev. (MMscf/d)	0.042	0.042
[1]Eq. 7, [2]Production Log, [3] $C_{fD}\big\vert_{ch} = (\pi/2)C_{fD}$		

The history match was based on two different scenarios for the choked skin: 1) no tail-in of high conductivity proppant where the choked skin is based on the history matched dimensionless conductivity $C_{fD}|_{ch} = C_{fD}$ and 2) a tail-in of high conductivity proppant where the dimensionless fracture conductivity for choked flow is estimated to be $C_{fD}|_{ch} = (\pi/2)C_{fD}$. Because of the higher permeability of the tail-in proppant and multi-clusters per stage that promote discrete fracture networks (DFN) and a greater SRV, we believe the fracture conductivity near the wellbore should be greater than the average fracture conductivity. A discrete fracture network geometry would also account for the short propped fracture lengths. Shorter propped lengths may also be attributed to proppant settling during shut-in. If the jobs are over flushed, this may hinder near wellbore conductivity unless the "halo effect" of an opened un-propped fracture in the near wellbore region does not extend too far into the formation.

Table 5 illustrates, as expected, that for a higher tail-in conductivity relative to the average fracture conductivity, the history match solution results in lower values for the formation permeability, choked skin, and average fracture conductivity and higher values for the propped length to minimize the error between predicted and measured flow rates. As illustrated, there are no unique history match solutions. Consequently, we will concentrate on the higher tail-in conductivity solution as being more realistic for typical fracture treatments pumped in most unconventional formations (i.e., proppant tail-ins with higher concentrations and greater permeabilities).

Figure 8 shows a history match of the measured gas flow rate and bottomhole flowing pressure data (199 data points over 201 days) with the numerical results. The history match analysis of measured and predicted flow rate was based on optimizing the following parameters for a high proppant conductivity tail-in: propped fracture half-length ($x_f = 363$ ft), dimensionless conductivity ($C_{fD} = 16$), choked skin ($S_{ch} = 0.067$), and formation permeability ($k = 478$ nD) as given in Table 5. The resulting reservoir capacity (kh) was calculated to be 0.077 mD-ft. The average error between the measured and predicted gas flow rates was 1.3% with a standard deviation of 0.042 MMscf/d.

A petrophysical analysis showed an average permeability of 377 nanodarcy (nD) over a formation thickness of 162 ft that included the Upper and Lower Marcellus. The resulting reservoir capacity (kh) was calculated to be 0.061 mD-ft. An After Closure Analysis (ACA) from a nearby well resulted in a pore pressure gradient of 0.62 psi/ft, an average reservoir permeability of 555 nD, and a reservoir capacity of 0.09 mD-ft. The history match results of this study match very well with these sources.

Although the production data was only for about 200 days, the predicted values for these parameters seem to be reasonable based on the fracture treatment, efficiency, and expected permeability for this unconventional shale play. Longer time data will provide a more accurate picture of the predicted results.

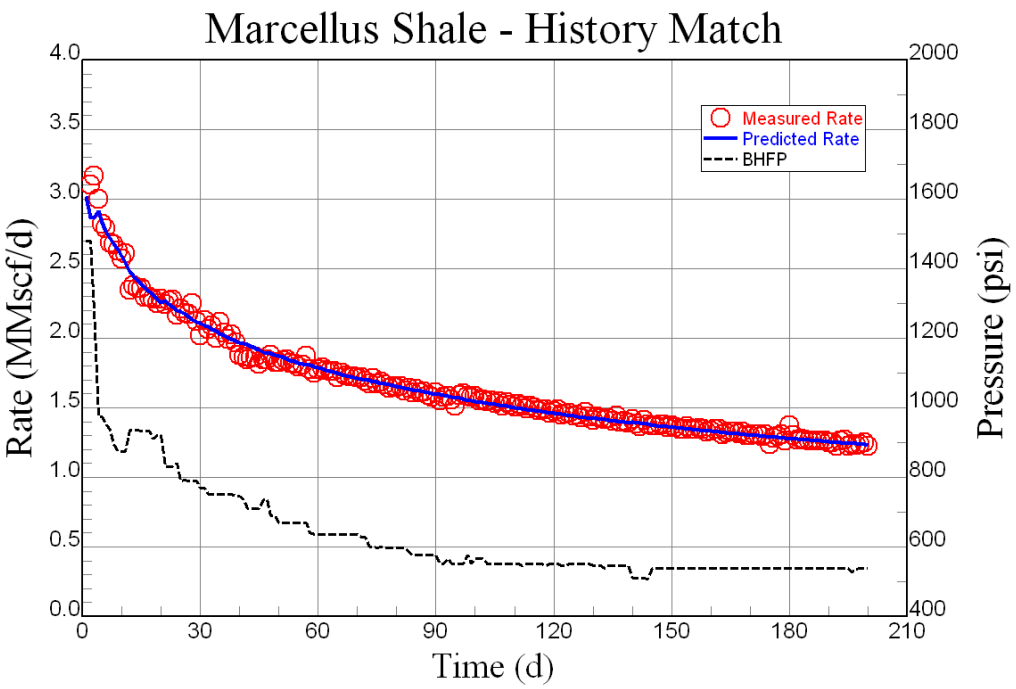

Fig. 8 — Marcellus Shale - History match of measured and predicted gas flow rate versus time for multiple transverse fractures.

Figure 9 shows the predicted gas flow rate based on the history match parameters for a period of ten years. This figure illustrates that it will take about ten years for the flow rate to decline to 10% of the initial production rate.

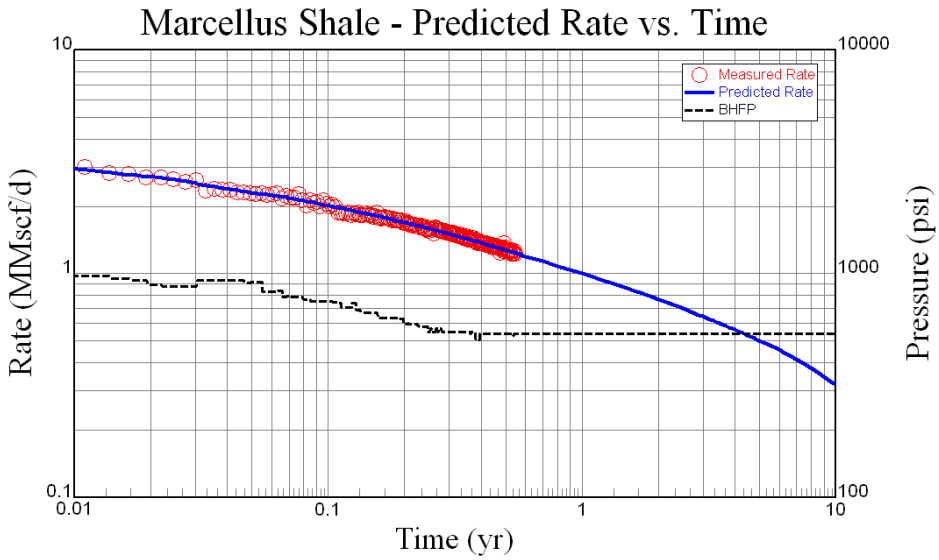

Fig. 9 — Marcellus Shale - Predicted and measured gas flow rate versus time for six multiple transverse fractures.

The predicted cumulative gas production as a function of time is shown in Figure 10. As illustrated, the cumulative production after one year will be about 0.5 Bscf. The 5 and 20 year cumulative production values will be about 1.5 Bscf and 3.0 Bscf, respectively.

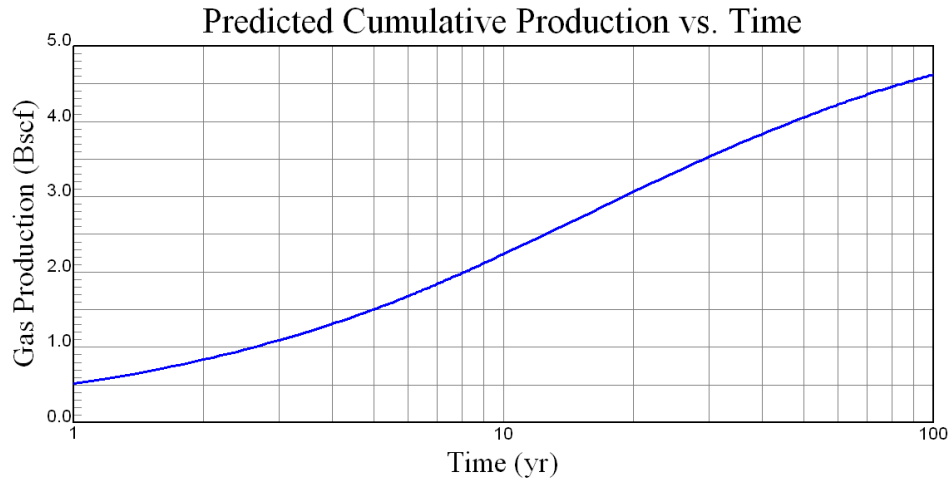

Fig. 10 — Marcellus Shale - Predicted cumulative production versus time for six multiple transverse fractures.

The EUR for this 80 acre drainage area as a function of the number of transverse fractures assuming all transverse fractures contribute and the fractures near the toe of the lateral cleanup is now investigated. The multiple transverse fractures are also assumed to be equally spaced throughout the reservoir with a higher proppant conductivity tail-in. The gas flow rate and cumulative production based on the history matched parameters in Table 5 for a constant BHFP of 530 psi as a function of the number of transverse fractures are shown in Figure 11 and Figure 12. Figure 11 illustrates that the time for interference decreases as the number of multiple transverse fractures increase within a given lateral length. However, since the formation diffusivity is moderate (3,300 mD-psi/cp) the transverse fracture spacing could be closer without substantial interference in the near term while maximizing the flow rate and cumulative production. The spacing for an interference time of three months with a diffusivity of about 3,300 mD-psi/cp is $\Delta y = (\eta t/237)^{1/2} \cong 175$ ft or about 21 equally spaced multiple transverse fractures (i.e., 21 equally spaced fractures within a reservoir of lateral length

y_e = 3,733 feet). The cumulative recovery after one year for 10 and 35 equally spaced transverse fractures is about 0.9 and 2.0 Bscf, respectively. As illustrated, the EUR for a drainage area of 80 acres can be maximized to about 5.5 Bscf by increasing the number of contributing transverse fractures. The economics for multi-stage/cluster spacing optimization must also be addressed as discussed below.

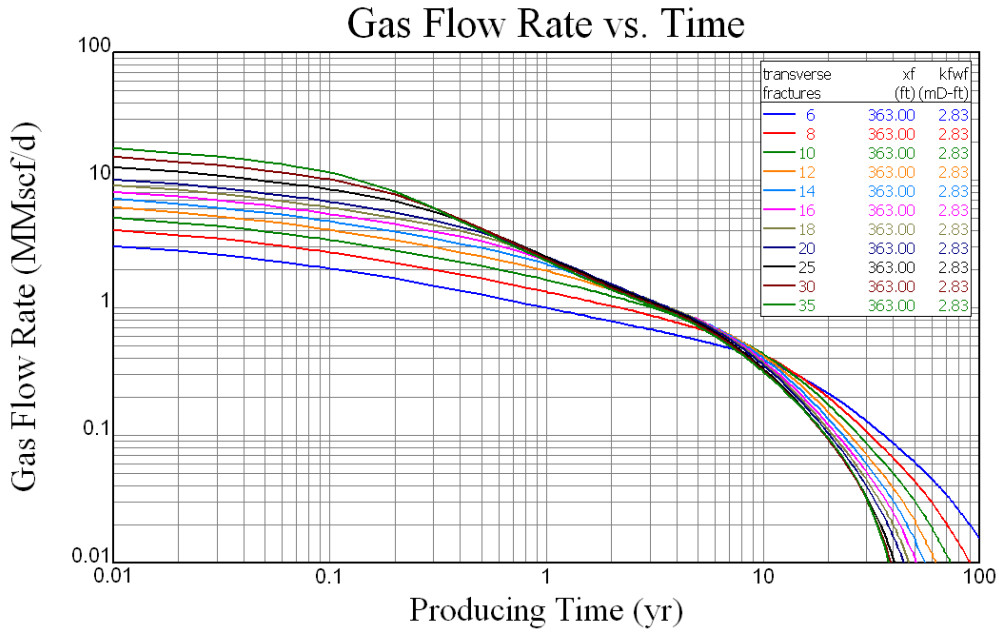

Fig. 11 — Marcellus Shale - Gas rate versus time for various multiple transverse fractures.

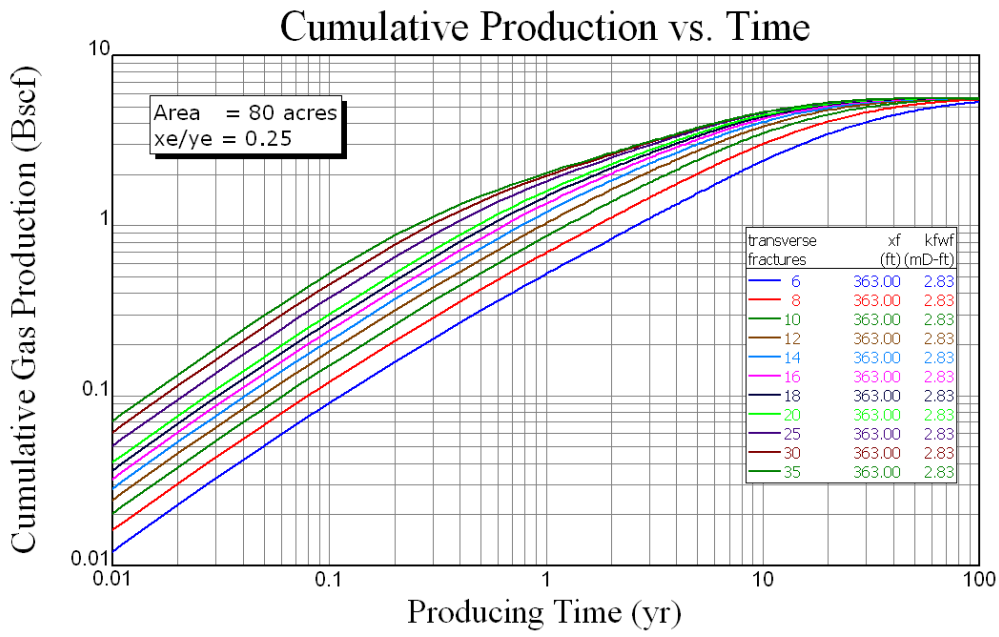

Fig. 12 — Marcellus Shale - Cumulative production versus time for various multiple transverse fractures.

Eagle Ford Shale - Case Study

The Eagle Ford formation is a widespread Upper Cretaceous deposit in the Gulf Coast region of South-Central Texas long known as a source rock for other plays. Only recently has it been recognized as an unconventional oil and gas play. In South Texas, where it has hydrocarbon potential, the Eagle Ford formation is between 5,000' and 13,000' below the surface and ranges in thickness from 50' to 300'. Although described as a shale, the Eagle Ford formation is actually composed of organic-rich calcareous mudstones and chalks that were deposited during two transgressive sequences (the

Upper and Lower Eagle Ford). Total organic carbon (TOC) in the Eagle Ford formation ranges from 1-7%. The organic richness in the Eagle Ford typically increases with depth. As such, the Lower Eagle Ford tends to be more organically rich and produces more hydrocarbons.

The calcareous makeup of this rock makes this play significantly different than other well-known unconventional plays such as the Barnett Shale, Haynesville Shale, and Marcellus Shale (all of which are found in primarily siliceous environments).

Because of the regional extent, the Eagle Ford formation consists of several different sub-plays within itself. In La Salle County, a sweet spot has been identified between the Edwards shelf edge and the Sligo shelf edge. The burial depth in this area ranges from 10,000' to 13,000' and has effectively created a mini-basin where the Eagle Ford accumulated an oxygen-deficient environment, which has resulted in wells that produce large quantities of dry gas. Further to the northwest, in the Maverick Basin, the Eagle Ford is much shallower (5,000' - 8,500') and may have provided an ideal depositional environment for Eagle Ford but this area did not reach the same level of hydrocarbon maturity as LaSalle County and, therefore, produces a much more condensate rich gas and potentially volatile oil in the shallowest areas. To the northeast, in Live Oak, Karnes, and DeWitt Counties (among others) the Eagle Ford is being explored primarily along the backside of the Edwards Reef. These areas generally produce a respectable amount of condensate along with gas.

The Eagle Ford well was completed with a ten stage stimulation using slickwater, linear gel, and ceramic proppant in a 4,000 foot lateral. Composite flow through bridge plugs was used for isolation and four two-foot clusters were perforated per stage (40 clusters total). The first and last intervals were shot at six (6) shots per foot (spf) and the middle two intervals were shot at 12 spf. The average treating rate and pressure was about 50 bpm and 8,900 psi, respectively. The proppant concentration for each stage increased from 0.25 to 1.5 lbm/gallon without slickwater sweeps. Linear gel was used to place 0.75 to 1.5 pound concentration of proppant. Average proppant placed per stage was ~250,000 lbm and 11,300 gallons of water. Production logs and chemical traces in the flowback samples indicated that all clusters have somewhat variable production rates; however, the total production from each fracture treatment stage are producing approximately equal volumes. As such, the production data history matched used forty (40) multiple transverse fractures (ten stages with four clusters per stage).

The Eagle Ford formation and history match results based on a ten stage, four clusters per stage transverse hydraulic fracture treatment in a horizontal well are given in Table 6. The Eagle Ford shale history matched parameters are given in Table 7.

Table 6. Eagle Ford - Reservoir and Fracture Properties.

Formation	Eagle Ford
Depth (ft)	10,875
Thickness (ft)	283
HC Porosity (%)	5.76
Pore Pressure (psi)	8350
Specific Gravity	0.621
Temperature ($^\circ F$)	285
Drainage Area (acres)	80
Aspect Ratio, $\lambda = x_e/y_e$	1/4
Reservoir Size (x_e, y_e), (ft)	(933.38, 3733.52)
Flowing BHP (psi)	3900-1500

Fracture/Wellbore	
Number of Stages	10
Clusters/Stage	4
Number Transverse Fracs	40
Lateral Length (ft)	4,000

Table 7. Eagle Ford - History Matched Parameters

Formation - Eagle Ford	No Tail-in	Tail-in
Permeability, k, (nD)	17.2	12.2
Reservoir Capacity, kh, (mD-ft)	0.0049	0.0035
Diffusivity, η, (mD-psi/cp)	153	109
Fracture		
Propped Length (ft)	131	157
Conductivity, $k_f w_f$, (mD-ft)	0.86	0.57

Table 7. Eagle Ford - History Matched Parameters

Formation - Eagle Ford	No Tail-in	Tail-in
Dim. Conductivity, C_{fD}	382	297
Choked Skin, [1] S_{ch}	0.0254	0.0173[3]
Number Equivalent Fracs[2]	40	40
Lateral Length[2] (ft)	4,000	4,000
Error (%)	2.2	2.1
Std. Dev. (MMscf/d)	0.088	0.085
[1]Eq. 7, [2]Production log, [3] $C_{fD}\big\vert_{ch} = (\pi/2)C_{fD}$		

The history match was based on two different scenarios for the choked skin as discussed for the Marcellus study: 1) no tail-in (uniform conductivity) and 2) a high permeability proppant tail-in. The results are similar to the Marcellus study in that for a high conductivity tail-in relative to the average fracture conductivity, the history match solution results in lower values for the formation permeability and average fracture conductivity and higher values for the propped length to minimize the error between predicted and measured flow rates, as expected.

Figure 13 shows a history match of the predicted and measured gas flow rate and bottomhole flowing pressure data with time for the tail-in case. The history matched parameters were: propped fracture half-length (x_f = 157 ft), dimensionless conductivity (C_{fD} = 297), formation permeability (k = 12.2 nD), and choked skin (S_{ch} = 0.0173), as given in Table 7. As discussed previously, the created discrete fracture network and large stimulated reservoir volume account for what appears to be a short fracture length. A gas shale core analysis (rotary sidewall core) was performed on nine crushed 20/35 mesh size samples. The analysis showed matrix permeabilities ranging from 1 to 200 nD with an arithmetic average of 68 nD for the sample set.

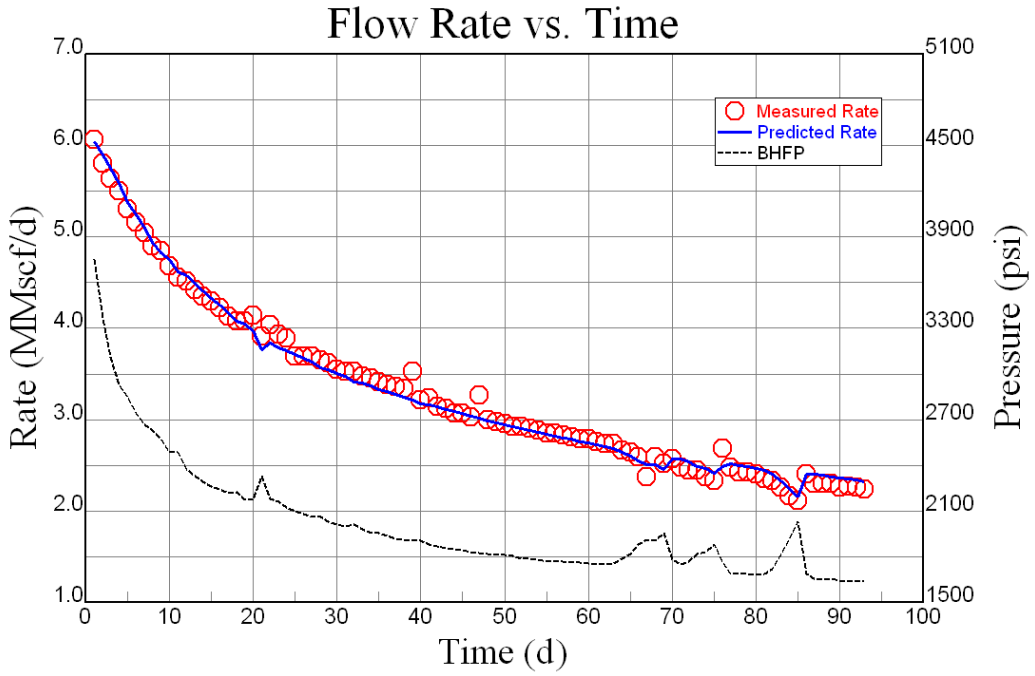

Fig. 13 — Eagle Ford Shale - History Match of gas flow rate versus time for 40 multiple transverse fractures.

Figure 14 shows the predicted gas flow rate based on the history match parameters for a period of ten years. As illustrated, it will take about four years for the production rate to decrease to 10% of its initial value.

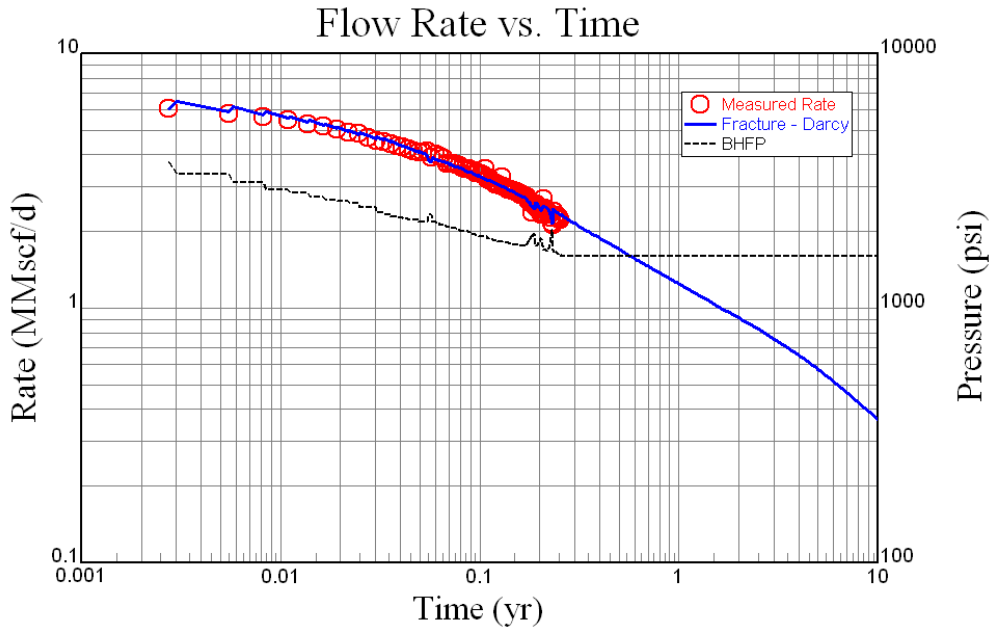

Fig. 14 — Eagle Ford Shale - Predicted and measured gas flow rate versus time for forty multiple transverse fractures.

The predicted cumulative gas production as a function of time is shown in Figure 15. As illustrated, the cumulative gas production after one and ten years of production will be about 0.75 and 2.7 Bscf, respectively.

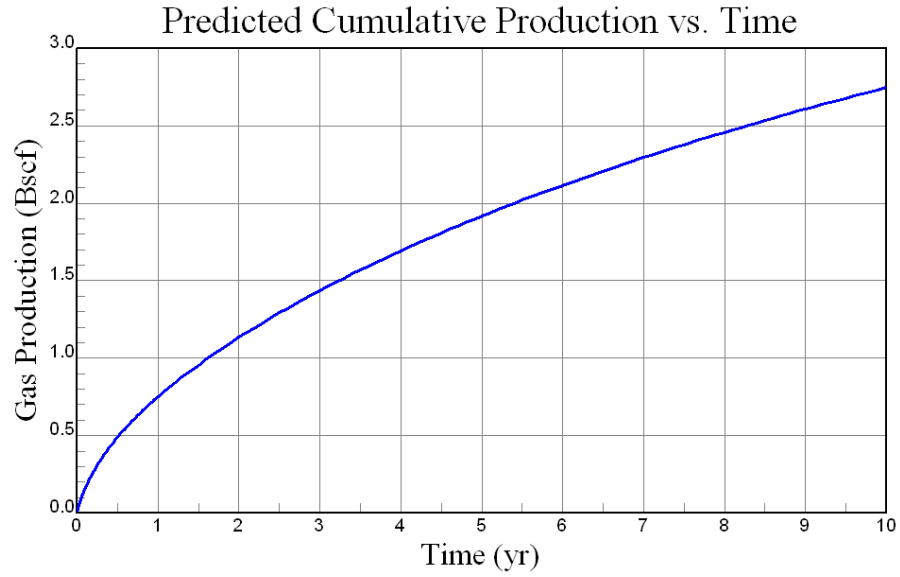

Fig. 15 — Eagle Ford Shale - Predicted cumulative production versus time for forty multiple transverse fractures.

The time for interference with a formation diffusivity of 109 mD-psi/cp and fracture spacing of 100 feet is $t = (237/\eta)\Delta y^2 \cong 2.5$ yr .

Optimization - Transverse Fractures in Horizontal Wells

Prats was the first to demonstrate that there is an optimum length-width ratio (dimensionless conductivity) for a given fracture volume that maximizes productivity. Prats showed that the optimum dimensionless conductivity for low penetrations was about 1.26 (i.e., $C_{fD} = \pi/(2a)$ where the optimum value for a was about 1.25 for an ellipsoidal shaped fracture). The optimum value for a was later refined and shown to be equal to unity (Economides and Nolte (1987)).

Economides *et al.* (2002), also showed there existed an optimum fracture design for a given propped fracture volume.

Their analysis was based on a dimensionless proppant number (N_{prop}) that was defined as twice the ratio of the propped fracture volume to reservoir volume multiplied by the fracture to reservoir permeability ratio.

Holditch *et al.* (1978) presented one of the first papers on the optimization of well spacing and fracture length in low permeability formations. Their objective was to present a simple technique for optimizing profit from a tight gas reservoir. Holditch performed sensitivity studies by varying such parameters as permeability, pay thickness, formation drainage area, propped fracture length, etc. Their analysis also included the variations on the economic parameters to determine the effect of gas price and discount rate upon the optimum results. Holditch concluded that "The values of the original pressure, porosity, net gas pay, drilling, completion and operating costs must all be considered to determine the optimum development plan for a given reservoir."

Elrafie and Wattenbarger (1997) also presented an early paper on the economic evaluation of a horizontal well with four transverse fractures producing from the Upper Bahariyia reservoirs. This is a multi-zone oil reservoir with a 2 to 6 mD permeability in the horizontal and 0.3 to 1 mD permeability in the vertical for two zones, respectively. They presented cash flow and net present value (NPV) profiles for the study in order to evaluate the economic feasibility of the horizontal well. Investments and expenses to drill, complete, fracture, and operate the well were considered. Their final conclusion was "In the Upper Bahariyia reservoirs: for a horizontal well with a length of 1500 feet, the optimum number of transverse fractures is 4 with fracture spacing of 300 feet."

The economic optimization methodology presented below is based on the concept of Net Present Value (NPV) and Discounted Return on Investment (DROI) as given in Appendix E. The objective of this study is to determine the optimum number of transverse fractures in a horizontal gas well for a hypothetical gas shale formation. The well, formation, and transverse fracture properties are given in Table 8. The economic inputs are given in Table 9.

Table 8. Shale Gas Study - Reservoir and Fracture Properties.

Formation - Shale Gas	
Depth (ft)	7,500
Thickness (ft)	75
Permeability (nD)	500
HC Porosity (%)	5
Pore Pressure (psi)	3,400
Temperature ($^\circ F$)	200
Gas Specific Gravity	0.65
Diffusivity (mD-psi/cp)	1864
Drainage Area (acres)	160
Aspect Ratio, $\lambda = x_e/y_e$	1/2
Flowing BHP (psi)	500

Wellbore/Fracture	
Wellbore Radius (ft)	0.333
Lateral Length (ft)	3,000
Propped Length (ft)	800
Conductivity, $k_f w_f$, (mD-ft)	20
Dim. Conductivity, C_{fD}	50
Choked Skin, [1] S_{ch}	0.00376[2]
Number Transverse Fracs	1-100

[1] Eq. 7

[2] $C_{fD}\big|_{ch} = (\pi/2)C_{fD}$

Table 9. Shale Gas Study - Economic Data.

Formation - Shale Gas	
Gas Unit Revenue ($/Mscf)	5
Inflation Rate (%)	0
Revenue Escalation (%)	0
Share of Cost (%)	100
Share of Revenue (%)	85
Cost/frac ($)	25,000
Well Cost ($)	2,000,000

The gas flow rate and cumulative production as a function of the number of transverse fractures with time is shown in Figure 16 and Figure 17. These figures illustrate that as the number of transverse fractures increases within a given lateral length, the time for interference decreases. For an interference time of one month with a diffusivity of 1,864 mD-psi/cp, the spacing is approximately 75 feet or about 40 transverse fractures over a 3,000 foot lateral (see Figure 35). The initial gas in place is about 6.5 Bscf with a cumulative recovery of about 4.4 Bscf (after 1,000 years!). The cumulative gas recovery after ten years of production for 20 or more multiple transverse fractures is shown to be about 3 Bscf. Clearly,

interference is a major factor in the decline rates and cumulative production after a few months.

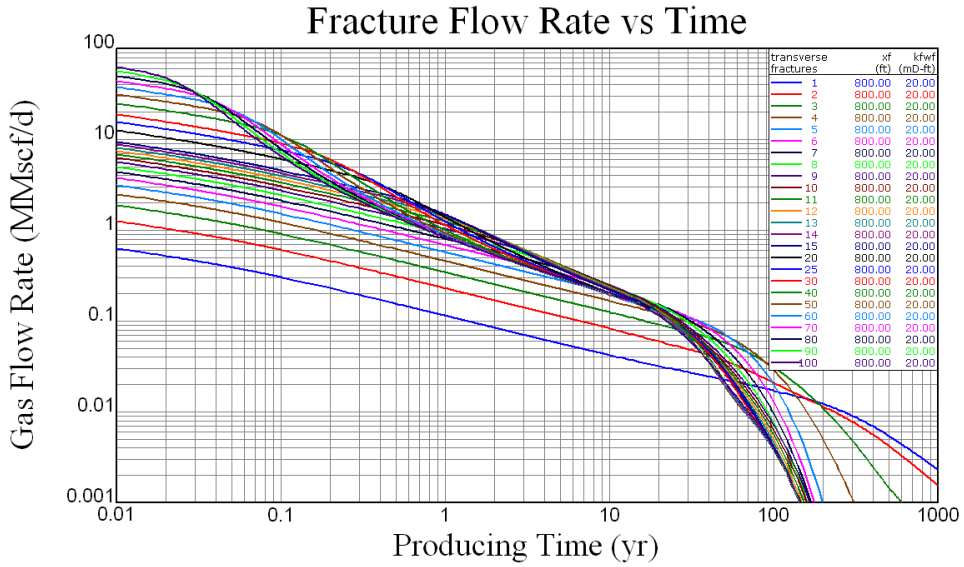

Fig. 16 — Shale Gas Study - Gas rate versus time for various multiple transverse fractures.

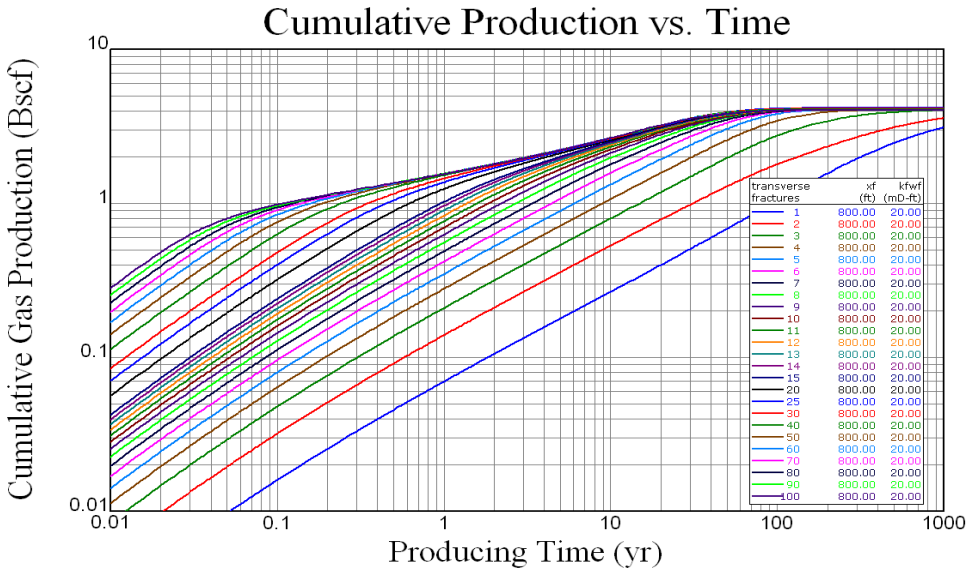

Fig. 17 — Shale Gas Study - Cumulative production versus time for various multiple transverse fractures.

Figure 18 and Figure 19 show the Net Present Value (NPV) and Discounted Return on Investment (DROI) as a function of the number of transverse fractures for selected times. Appendix E provides a summary of the economic relationships. In these studies, the total well cost was included as part of the stimulation costs. Figure 18 shows that as the NPV economic time for recovery increases the total number of optimum fractures decreases. After one year, the optimum number of transverse fractures is about 40, but if the economic recovery time increases to forty years, the optimum number of fractures over the 3,000 foot lateral would decrease to about 20. The net present value after three years is about $5.5 million for 30 fractures. Figure 19 illustrates that to maximize DROI, the optimum number of fractures ranges from about 30 for year one to about 10 for long term recovery. If the economics are based on the first year, the optimum number of fractures is about 30 with a DROI of 2.5 (i.e., for every dollar invested in drilling and fracturing a total return of $2.5 will be realized). Likewise, for an economic investment period of three years, the optimum number of fractures falls to about 20 with a DROI of 3.1.

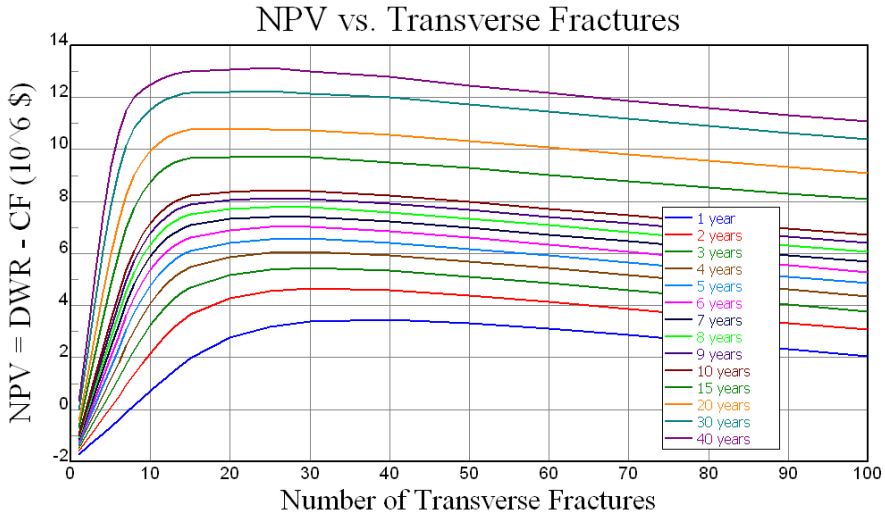

Fig. 18 — Shale Gas Study - Net Present Value (NPV) versus number of transverse fractures for selected times.

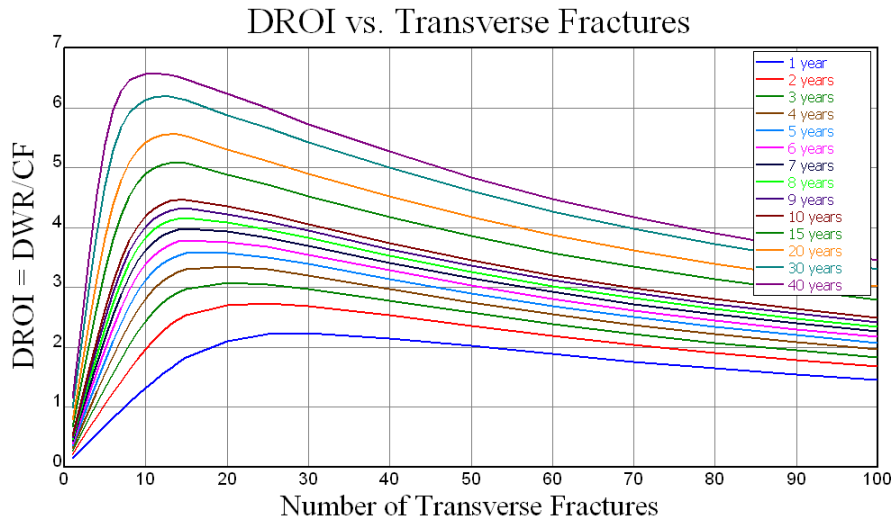

Fig. 19 — Shale Gas Study - Discounted Return on Investment (DROI) versus number of transverse fractures for selected times.

The above example illustrated the methodology to optimize the number of transverse fractures of a specified fracture length to maximize the NPV and DROI. An analysis is now presented to optimize the fracture length for a given pre-specified number of stages and clusters/stage. For this study, a total of ten stages with five clusters per stage (50 transverse fractures) were modeled with the object of optimizing fracture length. The choked skin was also based on a higher tail-in dimensionless conductivity as discussed above, where $C_{fD}\big|_{eh} = (\pi/2)C_{fD}$. To simplify the study, it was assumed the fracture treatment costs were an algebraic function of the job size as calculated from the parametric relationships of fracture characteristics given by Meyer (1986). The propped fracture length and width for a high efficiency (low fluid loss), well contained (little height growth) fracture are proportional to the injected volume by the relationships $L \propto V^{4/5}$ and $w_f \propto V^{1/5}$. The corresponding fracture conductivities are given by $k_f w_f \propto L^{1/4}$ and $C_{fD} \propto L^{-3/4}$.

The dimensionless conductivity and treatment costs versus fracture length are given in Figure 20 and Figure 21, respectively. As illustrated, the dimensionless fracture conductivity decreases and the treatment costs increase with a slight upward concavity for increasing propped fracture length. If height growth occurs or if the fracture system exhibits discrete fracture network behavior, the treatment costs would show a much steeper rate of increase with propped length.

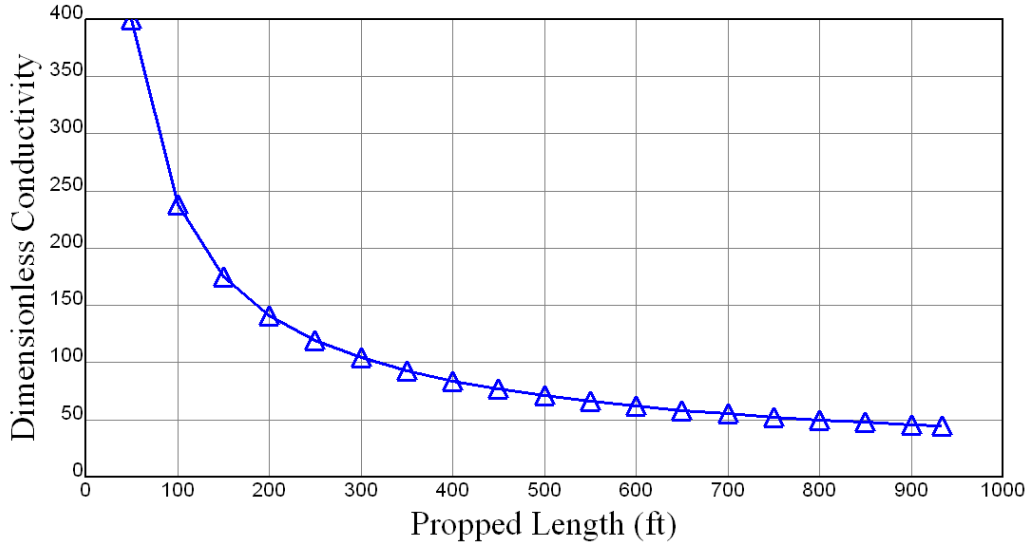

Fig. 20 — Shale Gas Study - Dimensionless fracture conductivity versus propped fracture length.

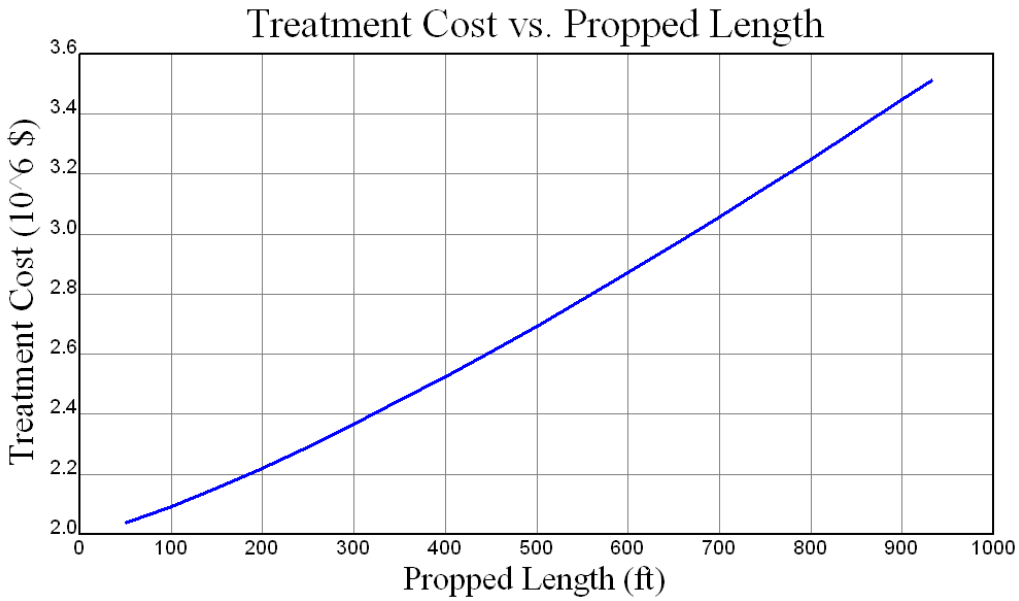

Fig. 21 — Shale Gas Study - Treatment cost versus propped fracture length - 10 stages with 5 clusters/stage.

The gas flow rate and cumulative production as a function of fracture length and time for various propped fracture lengths are shown in Figure 22 and Figure 23. As illustrated, as fracture length increases within the 3,000’ horizontal lateral the initial productivity and total gas recovery also increase as expected. The incremental productivity, however, is shown to decrease with increased incremental fracture length as a function of time.

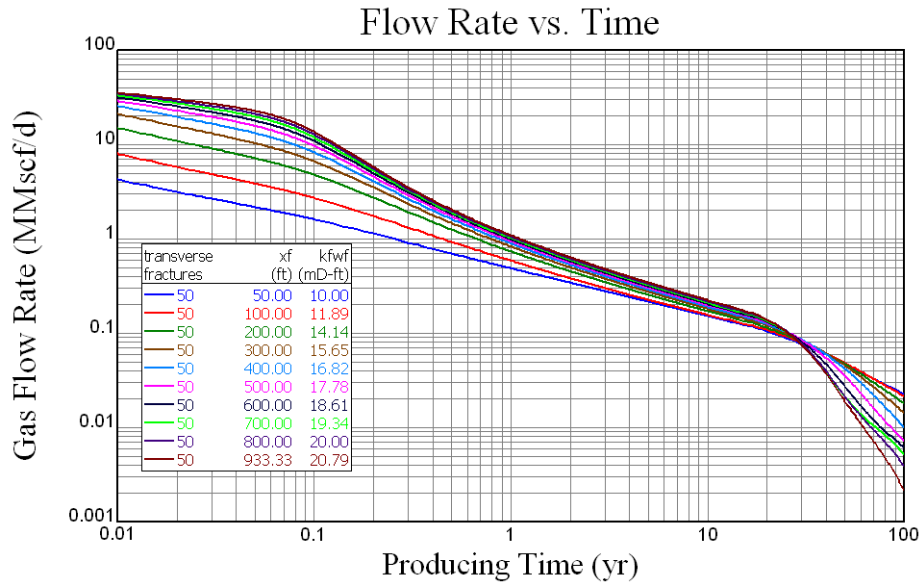

Fig. 22 — Shale Gas Study - Gas rate versus time for various propped lengths: 10 stages with 5 clusters/stage.

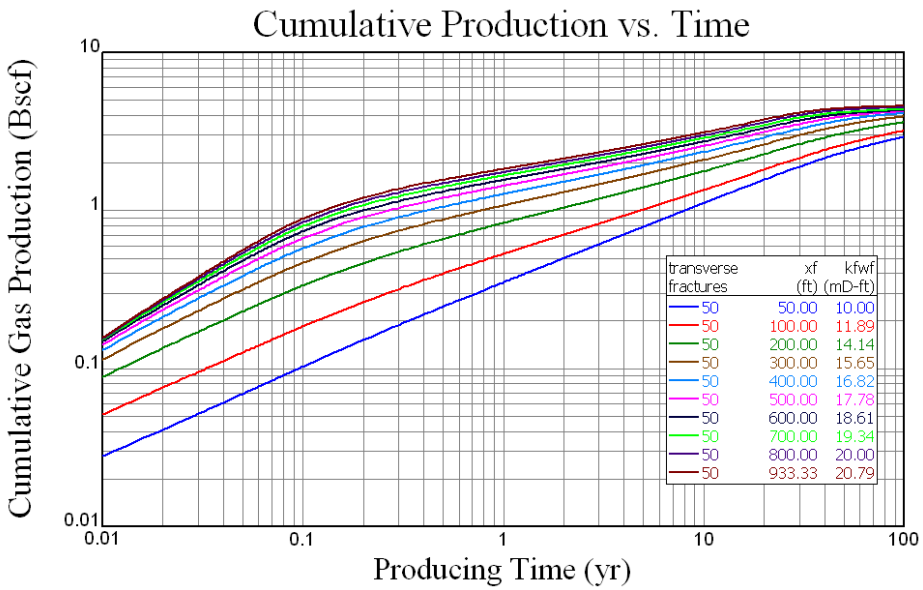

Fig. 23 — Shale Gas Study - Cumulative production versus time for various propped lengths:10 stages with 5 clusters/stage.

Figure 24 and Figure 25 show the Net Present Value (NPV) and Discounted Return on Investment (DROI) as a function of the propped fracture length for a ten stage treatment with five clusters/stage at selected times. Figure 24 illustrates that the maximum NPV is realized when the fracture length fully penetrates the formation (i.e., $I_x = x_f/x_e = 1$). Figure 25 shows that as the economic time for investment recovery increases the optimum DROI is realized for shorter propped fractures. That is, after one year the optimum propped fracture length is about 650 feet while for a five year period the optimum length is about 600 feet. The net present value after three years is about $6.1 million for a length of 800 feet and about $5.5 million for a propped fracture length of 600 feet. Figure 25 also illustrates that to maximize DROI the optimum propped fracture length for the first year is about 650 feet with a DROI of 2.3. The optimum fracture length for a ten year investment is 550 feet with a DROI of about 4.0.

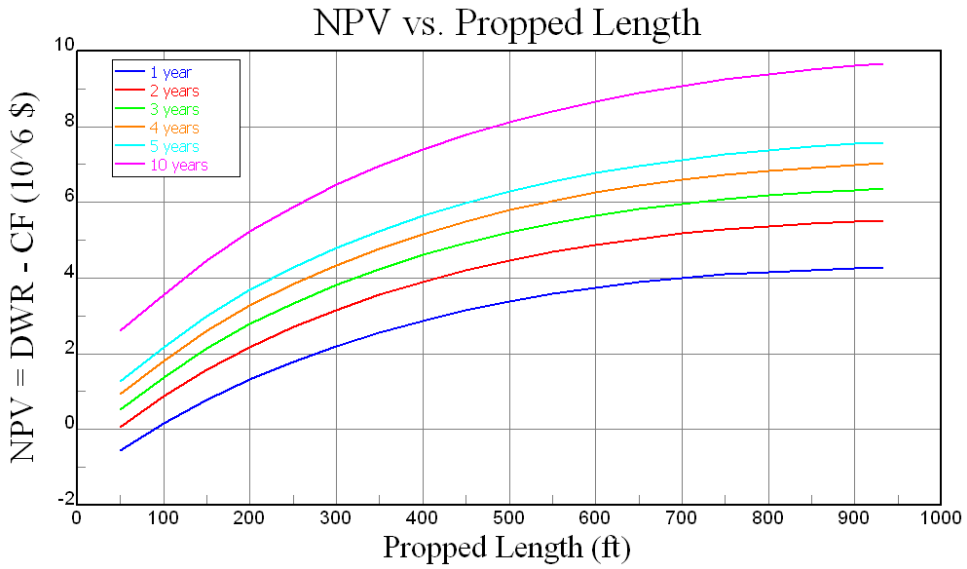

Fig. 24 — Shale Gas Study - Net Present Value (NPV) versus propped fracture length for selected times.

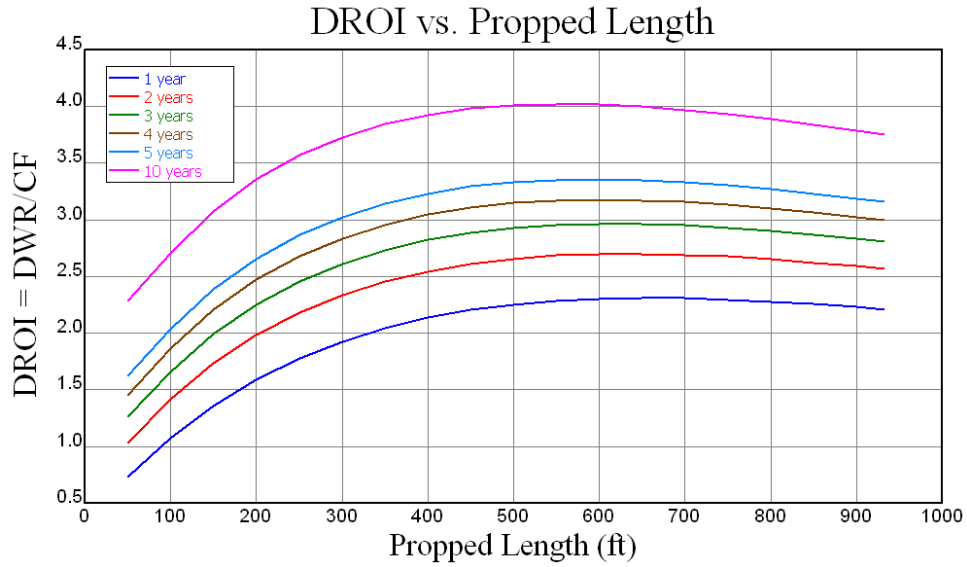

Fig. 25 — Shale Gas Study - Discounted Return on Investment (DROI) versus propped fracture length for selected times.

Conclusions

An analytical model for the optimization of multiple transverse fractures in horizontal wellbores has been presented. The numerical productivity solution is based on the trilinear model of Lee and Brockenbrough (1983, 1986) and the pseudosteady-state resistivity model of Meyer and Jacot (2005). The analytical results have demonstrated the ability to accurately model finite-conductivity vertical fractures in closed rectangular systems. A methodology of using these analytical solutions to formulate a set of fundamental dimensionless pressure and rate solutions for multiple stage/clusters transverse fractures in horizontal wells was presented. Although these solutions are not exact for all cluster/stage combinations, the analytical results compare very well with 3-D numerical gridded simulators.

In particular, a methodology based on Net Present Value (NPV) and Discounted Return on Investment (DROI) was presented to help the design engineer optimize the number of transverse fractures (number of stages and clusters/stage) and fracture length in horizontal wellbores.

The major conclusions and contributions are summarized below:

1. A mathematical model describing the production solution for multiple transverse finite-conductivity vertical fractures in horizontal wellbores was formulated. Numerous dimensionless pressure and rate solutions were given for various combinations of stage and cluster spacings.
2. Multiple transverse fracture rate performance and interaction (interference) were illustrated based on individual normalized interior and exterior rates versus time plots. The time for fracture interference as a function of formation diffusivity and fracture spacing was presented. The simple interference solution of Lee *et al.* ($t = 237\Delta y^2/\eta$) matches well with the numerical results of this paper. (Note: The diffusivity for gas formations should be based on average reservoir draw down values.) The normalized rate solutions presented follow the conclusions of Raghavan (1994) and Elrafie *et al.* (1994). That is, at early times all the individual fracture rates are the same and at late times the interior or central fractures produce at the lowest rates and the outermost or exterior fractures produce at the highest rates.
3. The analytical solution results were compared with the numerical results of a 3-D reservoir simulator for multiple transverse fractures intersecting horizontal wells in the Cotton Valley (gas shale) and the Bakken oil formations. These numerical results clearly illustrated that as the number of multiple transverse fractures increases, the total initial production (IP) increases linearly with the number of fractures, but because of interference the flow rate will decrease faster and at earlier times as the total number of multiple transverse fractures is increased over a given lateral length.
4. The history match and production data from the Marcellus and Eagle Ford formations demonstrated the importance of multiple transverse fracture optimization. Even though the production data sets were at early times, the analyses will help infer the fracture and reservoir characteristics for future design optimization. The current horizontal fracture methodology of closer spacings and more stages in very low (nanodarcy) shale plays may be justifiable from an engineering standpoint because of the large time for fracture interference.
5. The importance of utilizing Net Present Value (NPV) and Discounted Return on Investment (DROI) to optimize multiple transverse fractures in horizontal wellbores was illustrated. The economic methodology will help the design engineer optimize the number of stages/clusters and the fracture treatment (propped fracture length and conductivity) to maximize NPV and/or DROI. The economics, however, are clearly subject to current and future gas and oil prices, the specific formation properties (i.e., permeability, porosity, diffusivity, etc.), and the total stimulation costs (i.e., horizontal well drilling, lateral length, fracture treatment, etc.).
6. Hoping that the number/staging of multiple transverse fractures in a given horizontal wellbore are optimized is not a plan (i.e., In the words of Thomas Roehl: “Hope is not a plan.”). Currently, the industry is using a wide variety of engineering technologies to help optimize fracture treatments and increase profitability. The methodology presented in this paper will provide the engineer with a set of tools to make better and more informed decisions when optimizing fracture treatments in horizontal wellbores.

Nomenclature

a	=	Prats dimensionless inverse conductivity
A	=	Drainage area, L^2, ft^2
c	=	Constant of integration
c_t	=	Formation compressibility, Lt^2/m, 1/psi
C	=	Dimensionless conductivity parameter
C_A	=	Shape factor
C_{fD}	=	Dimensionless (net) fracture conductivity
f	=	Pseudo-skin function
g	=	Geometric parameter
h_f	=	Total fracture height, L, ft
h_p	=	Total pay zone height, L, ft
I_x	=	Fracture penetration ratio, x_f/x_e
J/J_0	=	Stimulation ratio
J_D	=	Dimensionless productivity ratio
k	=	Formation permeability, L^2, mD

k_f = Fracture permeability, L^2, mD
N_{prop} = Proppant number
p = Pressure, m/Lt^2, psi
p_i = Initial reservoir pressure, m/Lt^2, psi
$\bar{p}$ = Average reservoir pressure, m/Lt^2, psi
p_D = Dimensionless pressure
q = Flow rate, L^3/t, bpm or Mscf/d
q_D = Dimensionless rate
r_e = Equivalent drainage radius, L, ft
r_w = Wellbore radius, L, ft
r'_w = Effective wellbore radius, L, ft
S = Wellbore skin
S_{ch} = Choked fracture skin
S_f = Fracture skin
t = Time, t, hours
t_D = Dimensionless time
t_{DA} = Dimensionless time based on area
t_{Dx_f} = Dimensionless time based on fracture length
v = Velocity, L/t, ft/min
V_{res} = Reservoir volume, L^3, ft^3
w_f = Fracture width, L, ft
x_D = Dimensionless fracture position, x/x_f
x_e = Drainage half-length in x direction, L, ft
x_f = Fracture half-length, L, ft
y_e = Drainage half-length in y direction, L, ft

Greek

β_{x_e} = Geometric constant based on x_e
β_{r_e} = Geometric constant based on r_e
γ = Euler's constant, γ = 0.5772156649…
Δp = Differential pressure, m/Lt^2, psi
ΔS_f = Finite-conductivity fracture skin
ζ_∞ = Dimensionless effective wellbore radius for an infinite-conductivity fracture
η = Formation Diffusivity, L^2/t, mD-psi/cp
λ = Formation aspect ratio, x_e/y_e
μ = Reservoir viscosity, m/Lt, cp
ξ = Position, L, ft
ρ = Resistivity,1/ L, 1/ft
ϕ = Weight function or porosity
χ = Dimensionless inverse resistivity function
ψ = Laplace function
ω = Fracture flux distribution function

Subscripts

0 = Zero or wellbore
e = Effective or drainage

f	=	Fracture
r	=	Reservoir or radius
w	=	Well or width
wf	=	Flowing at well
x	=	Fracture position
∞	=	Infinite-conductivity
Superscript		
$\bar{}$	=	Average

Acknowledgement

The authors wish to thank Ms. Jessica L. and Kristin N. Meyer for thoroughly checking the accuracy of the cited references over their Christmas college break, and Michael Rozenfeld and Steve Lichlyter with Rosetta Resources for their assistance with the Eagle Ford formation description. We would also like to thank the management of Atlas Energy Resources, LLC., EQT Corporation, Chief Oil and Gas, Energy Corporation of America, and Rosetta Resources, Inc. for permission to publish the well data from the Marcellus and Eagle Ford shale formations.

References

Barker, B.J. and Ramey, H.J., Jr.: "Transient Flow to Finite Conductivity Vertical Fractures," SPE 7489, October 1978.

Bird, R.B., Stewart, W.E., and Lightfoot, E.N.: "Transport Phenomena," Wiley, New York, 1960, pp 5.

Brown, M., Ozkan, E., Raghavan, R., and Kazemi, H.: "Practical Solutions for Pressure Transient Responses of Fractured Horizontal Wells in Unconventional Reservoirs," SPE 125043, October 2009.

Cinco-Ley, H. and Samaniego-V: "Transient Pressure Analysis: Finite Conductivity Fracture Case versus Damaged Fracture Case," SPE 10179, October 1981.

Cinco-Ley: "Evaluation of Hydraulic Fracturing by Transient Pressure Analysis Methods," March 1982, SPE 10043.

Cinco-Ley, H., Samaniego-V, and Dominguez, A.N.: "Transient Pressure Behavior for a Well with a Finite-Conductivity Vertical Fracture," SPEJ August 1978.

Cinco-Ley, H., Ramey Jr., H.J, Samaniego-V, and Rodriguez, F.: "Behavior of Wells with Low-Conductivity Vertical Fractures," SPE 16776, September 1987.

Conlin, J.M., Hale, J.L., and Sabathier, J.C.: "Multiple-Fracture Horizontal Wells: Performance and Numerical Simulation," SPE 20960, October 1990.

Cooper, K.J. and Collins, R.E.: "Applications of Transient Pressure Interference Tests to Fractured and Nonfractured Injection Wells," SPE 19785, October 1989.

Earlougher, R.C., Jr. and Ramey, H.J., Jr.: "Interference Analysis in Bounded Systems," JCPT October-December 1973, 33-45.

Earlougher, R.C., Jr.: Advances in Well Test Analysis, Monograph Vol. 5, SPE, 1977.

Economides, M.J. and Nolte, K.G.: Reservoir Stimulation, Schlumberger Educational Services, Houston, Texas, 1987, pg. 11-3.

Economides, M.J., Delmbacher, Brand, C.W., and Helnemann, Z.E.: "Comprehensive Simulation of Horizontal-Well Performance," SPE Formation Evaluation, December 1991.

Economides, M., Oligney, R., and Valko, P.: Unified Fracture Design, Orsa Press, Alvin, Texas, 2002.

Elrafie, E.A. and Wattenbarger, R.A.: "Comprehensive Evaluation of Horizontal Wells with Transverse Hydraulic Fractures in the Upper Bahariyia Reservoirs," SPE 37759, March 1997.

Englander,T. and Lash, G.: "http://oilshalegas.com/marcellusshale.html", 2009.

Gidley, J.L., Holditch, S.A., Nierode, D.E., and Veatch, R.W.: Recent Advances in Hydraulic Fracturing, Monograph Vol. 12, SPE, 1989, pp 318.

Gilbert, J.V. and Barree, R.D.: "Production Analysis of Multiply Fractured Horizontal Wells," SPE 123342, April 2009.

Gringarten, A.C. and Ramey, H.J., Jr.: "The Use of Source and Green's Functions in Solving Unsteady-Flow Problems in Reservoirs," SPEJ, October 1973.

Gringarten, A.C., Ramey, H.J., and Raghavan, R.: "Unsteady-State Pressure Distributions Created by a Well with a Single Infinite-Conductivity Fracture," SPEJ, August 1974, 347-360.

Gringarten, A.C.: "Reservoir Limit Testing for Fractured Wells," SPE 7452, October, 1978.

Guo, G. and Evans, R.D.: "Pressure-Transient behavior and Inflow Performance of Horizontal Wells Intersecting Discrete Fractures," SPE 26446, October 1993.

Holditch, S.A.: "Quarterly Low-Permeability Gas Well Research Report for Fall," Petroleum Engineering Department, Texas A&M U., College Station, Texas, 1975.

Holditch, S.A., Jennings, J.W., and Neuse, S.H.: "The Optimization of Well Spacing and Fracture Length in Low Permeability Gas Formations," SPE 7496, October, 1978.

Horne, R.N. and Temeng, K.O.: "Relative Productivities and Pressure Transient Modeling of Horizontal Wells with Multiple Fractures," SPE 29891, March 1995.

Kustamsi, A., Hareland, G., Rampersad, P., and Permadi, P.: "Evaluation and Modification of Current Fractured Horizontal Well Inflow Models," SPE 39076, August 1997.

Larsen, L. and Hegre, T.M.: "Pressure Transient Behavior of Horizontal Wells With Finite-Conductivity Vertical Fractures," SPE 22076, May 1991.

Larsen, L. and Hegre, T.M.: "Pressure Transient Analysis of Multifractured Horizontal Wells," SPE 28389, Sept. 1994.

Lee, J. and Wattenbarger, R.A.: Gas Reservoir Engineering, SPE TextBook Series Vol. 5, 1996.

Lee, J., Rollins, J.B., and Spivey, J.P.: Pressure Transient Testing, SPE TextBook Series Vol. 9, 2003.

Lee, S.T. and Brockenbrough, J.R.: "A New Analytical Solution for Finite Conductivity Vertical Fractures with Real Time and Laplace Space Parameter Estimation," SPE 12013, October 1983.

Lee, S.T. and Brockenbrough, J.R.: "A New Approximate Analytical Solution for Finite-Conductivity Vertical Fractures," SPE Formation Evaluation, February 1986.

Lolon, E.P. and Mayerhofer, M.J.: "Application of 3-D Reservoir Simulator for Hydraulically Fractured Wells," SPE 110093, November 2007.

Lolon, E.P., Cipolla, C.L., Weijers, Hesketh, R.E., and Grigg, M.W.: "Evaluating Horizontal Well Placement and Hydraulic Fracture Spacing/Conductivity in the Bakken Formation, North Dakota," SPE 124905, October 2009.

Malekzadeh, D. and Tiab, D.: "Interference testing of Horizontal Wells", SPE 22733, October 1991.

McGuire, W.J. and Sikora, V.J.: "The Effect of Vertical Fractures on Well Productivity," SPEJ Vol. 219 401-403, 1960.

Medeiros, F., Kurtoglu, B., Ozkan, E., and Kazemi, H.: "Analysis of Production Data From Hydraulically Fractured Horizontal Wells in Tight, Heterogeneous Formations," SPE 110848, November 2007.

Meehan, D.N., Horne, R.N., and Ramey, H.J. Jr.: "Interference Testing of Finite Conductivity Hydraulically Fractured Wells," SPE 19784, October 1989.

Meyer, B.R.: "Design Formulae for 2-D and 3-D Vertical Hydraulic Fractures: Model Comparison and Parametric Studies," SPE 15240, May 1986.

Meyer, B.R. and Jacot, R.H.: "Pseudosteady-state Analysis of Finite Conductivity Vertical Fractures," SPE 95941, October 2005.

Mousli, N.A., Raghavan, R., Cinco-Ley, H., and Samaniego-V, F.: "The Influence of Vertical Fractures Intercepting Active and Observation Wells on Interference Tests," SPEJ, December 1982, 933-944.

Mukherjee, H. and Economides, M.J.: "A Parametric Comparison of Horizontal and Vertical Well Performance," SPE Formation Evaluation, June 1991.

Oasis Petroleum, LLC.: "Final Report of Stimulation Considerations for the Bakken," December 16, 2008.

Prats, M.: "Effect of Vertical Fractures on Reservoir Behavior - Incompressible Fluid Case," SPEJ, June 1961, 105-118.

Prats, M., Hazebroek, P., and Strickler, W.R.: "Effect of Vertical Fractures on Reservoir Behavior - Compressible-Fluid Case," SPEJ, June 1962, 87-94.

Raghavan, R.: "Pressure Behavior of Wells Intercepting Fractures," Proceedings, Invitational Well-Testing Symposium,

Oct. 19-21, 1977, 117-160.

Raghavan, R. and Hadinoto, Nico: "Analysis of Pressure Data for Fractured Wells: The Constant-Pressure Outer Boundary," SPEJ, April 1978, 139-149

Raghavan, R., Chen, C.C., and Agarwal, B.: "An Analysis of Horizontal Wells Intercepted by Multiple Fractures," SPE 27652, March 1994.

Ramey, H.J. and Cobb, W.M: "A General Pressure Buildup Theory for a Well in a Close Drainage Area," JPT December, 1971, 1493-1505.

Raymond, L.R. and Binder, G.G.: "Productivity of Wells in Vertically Fractured, Damaged Formations," JPT, Jan. 1967, 120-130.

Riley, M.F., Brigham, W.E., and Horne, R.N.: "Analytical Solutions for Elliptical Finite-Conductivity Fractures," SPE 22656, October 1991.

Russel, D.G. and Truitt, N.E.: "Transient Pressure Behavior in Vertically Fractured Reservoirs," JPT, October 1964, 1159-1170.

Scott, J.O.: "The Effect of Vertical Fractures on Transient Pressure Behavior of Wells," JPT, December 1963, 1365-1369.

Soliman, M.Y., Hunt, J.L., and El Rabaa, W.: "On Fracturing Horizontal Wells," SPE 18542, November 1988.

Stehfest, H: "Numerical Inversion of Laplace Transforms," Comm. ACM 13, 47-49, 1970.

Stevens, W.F. and Thodos, G.: "Prediction of Approximate Time of Interference Between Adjacent Wells," Trans. AIME, 1959, 216, 77.

Tinsley, J.M., Williams, J.R., Tiner, R.L., and Malone, W.T.: "Vertical Fracture Height - Its Effect on Steady-State Production Increase," JPT, May 1969, 633-638.

T.T. & Associates, Inc.: http://www.petrostudies.com/exoduspdf.pdf., December 2009.

Valko, P.P. and Economides, M.J.: "Heavy Crude Production from Shallow Formations: Long Horizontal Wells Versus Horizontal Fractures," SPE 50421, November 1998.

van Kruysdijk, C.P.J.W. and Dullaert, G.M.: "A boundary Element Solution To The Transient Pressure Response of Multiply Fractured Horizontal Wells," 2nd European Conference on the Mathematics of Oil recovery, Cambridge, 1989.

Vela, S. and McKinley, R.M.: "How Areal Heterogeneities Affect Pulse-Test Results", SPE 2569, July 1969.

Warren, J.E. and Hartsock, J.H.: "Well Interference," JPT, September 1960, 89-91.

Yost II, A.B. II, Overbey, W.K., Jr.: "Production and Stimulation Analysis of Multiple Hydraulic Fracturing of a 2,000-ft Horizontal Well," SPE 19090, June 1989.

Appendix A: Dimensionless Parameters

The following dimensionless parameters are used throughout this paper. The dimensionless pressure (p_D) for a constant production rate (q) is defined as

$$p_D = \frac{2\pi kh}{q\mu}\Delta p \tag{A.1}$$

where k is the formation permeability, h is the formation height, μ is the reservoir viscosity, and $\Delta p = p_i - p_{wf}$ is the differential pressure (the initial reservoir pressure (p_i) minus the flowing pressure (p_{wf})).

The dimensionless times based on the drainage area, A, wellbore radius, r_w, and fracture half-length, x_f, are defined as

$$t_{DA} = \frac{kt}{c_t\phi\mu A},\ t_D = \frac{kt}{c_t\phi\mu r_w^2},\ \text{and}\ t_{Dx_f} = \frac{kt}{c_t\phi\mu x_f^2} \tag{A.2}$$

where ϕ is the formation porosity and c_t is the formation compressibility.

The dimensionless rate (q_D) for a constant flowing pressure (p_{wf}) is defined as

$$q_D = \frac{\mu}{2\pi kh\Delta p}q(t) \tag{A.3}$$

The flow rate as a function of the dimensionless rate is

$$q(t) = \frac{2\pi kh\Delta p}{\mu} \cdot q_D \tag{A.4}$$

where $\Delta p = p_i - p_{wf}$ is the constant draw down pressure.

The productivity index (J) is defined as

$$J = \frac{q}{\bar{p} - p_{wf}} = \frac{2\pi kh}{\mu} J_D \tag{A.5}$$

where q is the flow rate, $\bar{p}$ is the average reservoir pressure, and p_{wf} is the flowing pressure. The dimensionless productivity index, J_D, is defined as

$$J_D = \frac{\mu}{2\pi kh} \cdot J = \frac{\mu}{2\pi kh} \cdot \frac{q}{\bar{p} - p_{wf}} \tag{A.6}$$

The dimensionless and Laplace parameters used in the production model are

$$C_{fD} = \frac{k_f w_f}{k x_f},\ C_D = \frac{C}{2\pi\phi c_t h r_w^2},\ C_{Df} = \frac{C}{2\pi\phi c_t h x_f^2}, \tag{A.7}$$

$$C_1 = \eta/\eta_f,\ \eta = k/(\phi\mu c_t),\ \eta_f = k_f/(\phi\mu c_t)_f, \tag{A.8}$$

$$S_f = \frac{\pi}{2}\frac{y_s}{x_f}\left(\frac{k}{k_s} - 1\right), \tag{A.9}$$

$$a = \frac{2}{C_{fD}},\ b = \frac{-\pi}{C_{fD}} \tag{A.10}$$

Appendix B: Governing Equations

The production solution for fractured wells is based on a finite-conductivity vertical fracture model. The analytical method developed couples the short time solution of Lee and Brockenbrough (1983, 1986) with the well known semi-log asymptotic (pseudo-radial) solutions of Ramey *et al.* The solution is applicable for all flow regimes from linear, bilinear, trilinear, and pseudo-radial.

The numerical solution allows for either a rate or pressure boundary condition at the well. Using the principle of superposition, a series of rates or pressures may be specified. For closed systems, the concept of desuperposition has been incorporated. Available for use with either gas or liquid, the numerical solutions have been improved for low conductivity fractures using the pseudosteady-state solution methodology of Meyer and Jacot (2005). The transition from trilinear to pseudo-radial flow is calculated in Laplace space.

Presented below are the fundamental solutions for the trilinear and pseudosteady-state solutions.

Trilinear Solution

The trilinear solution given by Lee and Brockenbrough (1983, 1986) for a finite-conductivity fracture in Laplace space is

Constant Rate

$$p_D(s) = \frac{b}{s(sbC_{Df} - \psi\tanh\psi)} \tag{B.1}$$

Constant Pressure

$$q_D(s) = \frac{1}{s^2 p_D(s)} = -\frac{\psi}{sb}\tanh\psi \tag{B.2}$$

The ψ parameter used in the above equations is defined by

$$\psi = \sqrt{\frac{a(s + s^{1/2})^{1/2}}{1 + (s + s^{1/2})^{1/2} S_f} + C_1 s} \tag{B.3}$$

This analytical solution is based on transforming the above equations from Laplace space to real time using the Stehfest inversion algorithm (1970).

Pseudosteady-State Equations

Ramey *et al.* (1971) defined pseudosteady-state as the condition in a finite closed reservoir when producing at a constant rate that "every point within the reservoir will eventually experience a constant rate of pressure decline." Ramey also states "That this condition has been referred to as pseudosteady, quasi-steady, semi-steady, and even steady state in the literature."

Dimensionless Pressure

Ramey *et al.* (1971), Earlougher and Ramey (1973), and Gringarten *et al.* (1974) showed that at sufficiently large producing times the system (unfractured or fractured) eventually reaches pseudosteady-state and the dimensionless pressure may be evaluated from

$$p_D(t_{DA}) = \frac{2\pi kh}{\mu q}(p_i - p_{wf}) = 2\pi t_{DA} + 1/J_D \tag{B.4}$$

Ramey (1971) showed that for pseudosteady-state flow

$$2\pi t_{DA} = \frac{2\pi kh}{\mu q}(p_i - \bar{p}) \text{ and } 1/J_D = \frac{2\pi kh}{\mu q}(\bar{p} - p_{wf}) = 1/2\ln\left(\frac{4A}{e^{\gamma} C_A r_w'^2}\right) \tag{B.5}$$

where C_A is the shape factor and r_w' is the effective wellbore radius as originally proposed by Prats (1961).

Effective Wellbore Radius

Rearranging Eq. B.5 in terms of effective wellbore radius, we have

$$\frac{1}{J_D} = \ln\left(\frac{4}{\sqrt{\lambda e^{\gamma} C_A(\lambda)}}\frac{x_e}{x_f}\right) + \ln\frac{x_f}{r_w'} \tag{B.6}$$

where the reservoir area for a rectangular reservoir $A = \pi r_e^2 = 4x_e y_e = 4x_e^2/\lambda$ has been incorporated.

The effective wellbore radius, r_w', concept was first introduced by Prats (1961, 1962) as a means to define an equivalent reservoir with wellbore radius, r_w', that would have a production behavior similar to that of a fractured reservoir. Prats showed that for high conductivity fractures ($C_{fD} \to \infty$) and small fracture penetration ratios ($x_f/x_e \to 0$), the effective wellbore radius was given by

$$r_w' \to x_f/2 \tag{B.7}$$

The effective wellbore radius concept is discussed in greater detail below as it pertains to finite and infinite-conductivity vertical fractures in closed systems.

Pseudo-Skin Relationships

The productivity index can be written in the form

$$\frac{1}{J_D} = \ln\left(\sqrt{\frac{4\pi}{e^{\gamma} C_A}}\frac{r_e}{x_f}\right) + f = \ln\left(\sqrt{\frac{4\pi}{e^{\gamma} C_A}}\frac{r_e}{r_w}\right) + S_f \tag{B.8}$$

where f is the pseudo-skin function with respect to the fracture half-length (x_f) and S_f is the fracture skin.

The relationships between the pseudo-skin function, f, dimensionless reciprocal effective wellbore radius, x_f/r_w', and fracture skin, S_f, are given below

$$f = \ln\frac{x_f}{r_w'} = S_f + \ln\frac{x_f}{r_w},\ S_f = \ln\frac{r_w}{r_w'},\ \frac{x_f}{r_w'} = e^f = \frac{x_f}{r_w}e^{S_f} \text{ and } r_w' = r_w e^{-S_f} = x_f e^{-f}. \tag{B.9}$$

Pseudosteady-State Resistivity Model

The mathematical formulation for a finite-conductivity vertical fracture in a closed rectangular system is based on the two-region domain resistivity model of Meyer and Jacot (2005) as shown in Figure 26.

The general definition for resistivity, ρ, is

$$\rho(\xi) \equiv -\frac{2\pi kh}{\mu q}\frac{dp}{d\xi} = \frac{\omega(\xi)}{\frac{A}{2\pi h}\frac{k(\xi)}{k}} \tag{B.10}$$

where $k(\xi)$ is the permeability as a function of position and k is the reference or far field reservoir permeability. The flow

rate as a function of position is given by $\omega(\xi) = q(\xi)/q(0)$ and is considered a dimensionless flux (e.g., see Bird *et al.* (1960)).

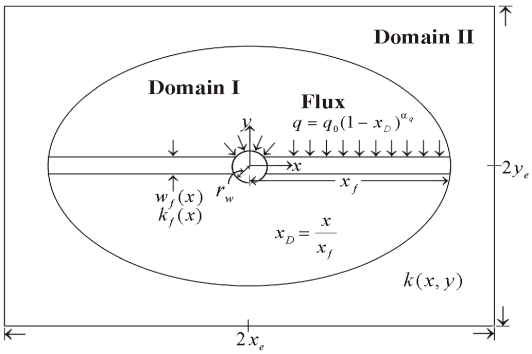

Fig. 26 — Schematic of a finite-conductivity vertical fracture in a rectangular reservoir.

The inverse dimensionless productivity index $(1/J_D)$ for finite (and infinite) conductivity fractures is found by integrating the resistivity over the flow domain as given by

$$\frac{1}{J_D} = \int_{\xi_0}^{\xi} \rho(\xi) d\xi + c \tag{B.11}$$

where ρ is the effective domain resistivity and c is the constant of integration.

The inverse dimensionless productivity index and other related equations for a piece-wise continuous linearly varying fracture conductivity in a homogeneous reservoir are summarized by Meyer and Jacot (2005).

One very important and fundamental solution for the dimensionless productivity index, J_D, is for the case of a finite-conductivity fracture of constant width and permeability (conductivity) in a homogeneous reservoir.

The general inverse productivity index is given by

$$\frac{1}{J_D} = \ln\left(\beta_{x_e} \frac{x_e}{x_f}\right) + f \tag{B.12}$$

The pseudo-skin function, f, and the reciprocal effective wellbore radius ratio, x_f/r'_w, for a uniform finite-conductivity fracture are

$$f = \ln\left[\left(\frac{\pi}{C_{fD} g(\lambda)} + \zeta_\infty\right) \Big/ \left(\frac{\pi}{C_{fD} g(\lambda)} \frac{r_w}{x_f} + 1\right)\right] \text{ and } \frac{x_f}{r'_w} = \left(\frac{\pi}{C_{fD} g(\lambda)} + \zeta_\infty\right) \Big/ \left(\frac{\pi}{C_{fD} g(\lambda)} \frac{r_w}{x_f} + 1\right) \tag{B.13}$$

where $g(\lambda)$ is a geometric parameter that is a function of aspect ratio and fracture conductivity (note: for a square reservoir $g(\lambda = 1) = 1$). The effective wellbore radius (i.e., reciprocal effective wellbore radius) for an infinite-conductivity fracture is defined as

$$\zeta_\infty \equiv x_f/r'_w\big|_{C_{fD} \to \infty} = e^{1/J_D} I_x / \beta_{x_e}(\lambda) \tag{B.14}$$

where the dimensionless productivity index J_D is found from Gringarten's closed form analytical pseudosteady-state solution and $\zeta_\infty(I_x)$ is a function of the penetration ratio ($I_x = x_f/x_e$).

The above equations can be simplified if the fracture permeability is much greater than the formation permeability, $k_f/k \gg 1$, and, if as is customary, it is assumed that fluid entering the wellbore comes only through the fracture. The resulting inverse productivity index upon simplifying Eq. B.15 with the above assumptions is

$$\frac{1}{J_D} = \ln\left(\beta_{x_e} \frac{x_e}{x_f}\right) + \ln\left(\frac{\pi}{C_{fD} g(\lambda)} + \zeta_\infty\right) \tag{B.15}$$

where the dimensionless fracture conductivity, C_{fD}, for $k_f/k \gg 1$ is approximated by $C_{fD} \cong k_f w_f/(k x_f)$.

Consequently, the above simplification is not appropriate for low-conductivity fractures and the more general form as given by Meyer and Jacot (2005) must be used.

The reciprocal effective wellbore radius ratio, x_f/r'_w, and pseudo-skin function, f, for a uniform finite-conductivity

fracture from Eq. B.13 are

$$f = \ln\left(\frac{\pi}{C_{fD}g(\lambda)} + \zeta_\infty\right) \text{ and } x_f/r_w' = \frac{\pi}{C_{fD}g(\lambda)} + \zeta_\infty . \tag{B.16}$$

Comparisons - Infinite Reservoir

A comparison of this model for a uniform finite-conductivity fracture in an infinite homogeneous reservoir with the pseudosteady-state solutions of Cinco-Ley (1982), Barker and Ramey (1978), Valko *et al.* (1998), and Riley *et al.* (1991) is presented.

The governing dimensionless pressure equation for an infinite system in terms of a pseudo-skin function, f, is

$$p_D = \frac{1}{2}\ln\left(\frac{4}{e^\gamma}t_{Dx_f}\right) + f(C_{fD}) \tag{B.17}$$

where f is a function of fracture conductivity (C_{fD}). The pseudo-skin functions reported by Gringarten *et al.* (1974) for a uniform-flux and an infinite-conductivity fracture are $f = 1$ and $f \cong \ln 2$, respectively.

The pseudo-skin function, f, and reciprocal effective wellbore radius, x_f/r_w', for a uniform finite-conductivity fracture in a homogeneous infinite reservoir ($\lambda = 1$, $g(\lambda) = 1$, and $\zeta_\infty = 2$) are

$$f = \ln(\pi/C_{fD} + 2) \text{ and } x_f/r_w' = \pi/C_{fD} + 2 . \tag{B.18}$$

Figure 27 shows the effective dimensionless wellbore radius as a function of fracture conductivity. A comparison of our analytical solution (assuming a constant fracture flux) with the work of Barker and Ramey (1978), Cinco-Ley (1982), Riley (1991) and Economides (2002) illustrates the excellent agreement. Figure 27 also shows that our constant conductivity solution (Eq. B.18) follows more closely with the results of Barker and Economides and the ellipsoidal form of our solution matches the results of Cinco-Ley and Riley.

Figure 28 shows the dimensionless pseudo-skin (Eq. B.18) for a constant conductivity and an ellipsoidal formulation as a function of dimensionless fracture conductivity. A comparison with the work of Barker and Ramey, Cinco-Ley *et al.*, Riley *et al.* and Economides *et al.*, is shown.

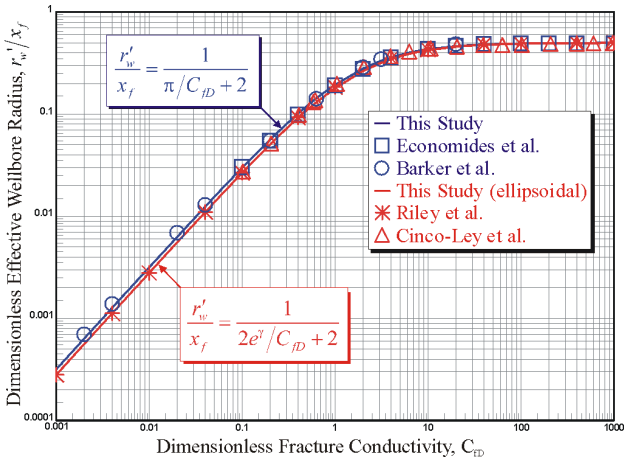

Fig. 27 — Dimensionless effective wellbore radius for a finite-conductivity vertical fracture - Comparison with the work of Economides, Barker, Cinco-Ley, and Riley *et al.*

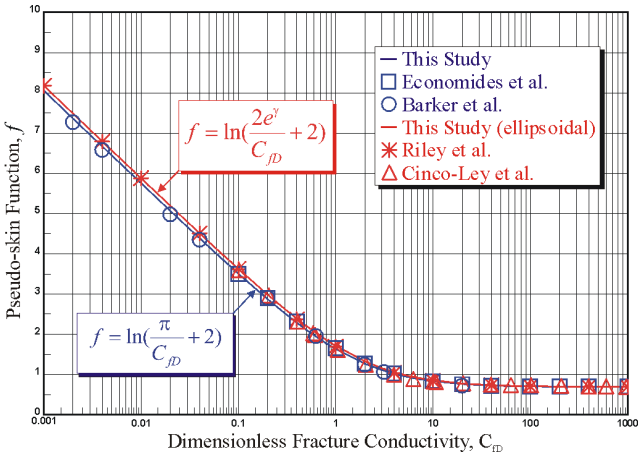

Fig. 28 — Pseudo-skin function versus dimensionless conductivity - Comparison with the work of Economides, Barker, Cinco-Ley, and Riley *et al.*

Comparison with Valko, Holditch, and McGuire et al.

Valko and Economides (1998) presented numerical pseudosteady-state solutions for finite-conductivity fractures in rectangular reservoirs.

Figure 29 shows a comparison of our model (Eq. B.15) with the published data of Holditch (1975, Gidley *et al.* 1989), McGuire and Sikora, and Valko *et al.* for the fracture performance (in terms of the productivity index) as a function of dimensionless fracture conductivity and penetration for a square reservoir ($\lambda = x_e/y_e = 1$). Figure 30 shows a similar comparison with Valko for a reservoir with an aspect ratio of ten, $\lambda = x_e/y_e = 10$.

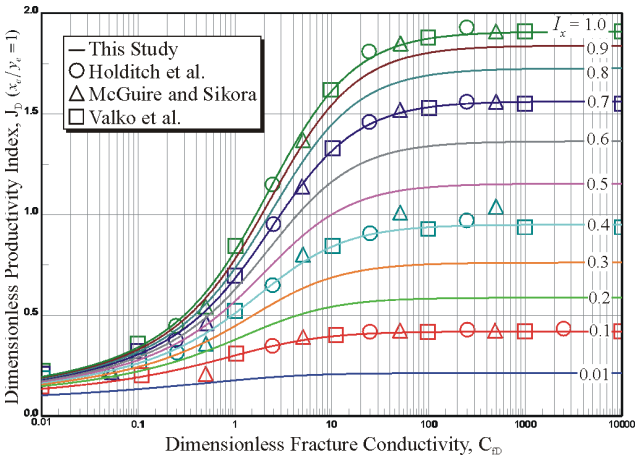

Fig. 29 — Dimensionless productivity index as a function of dimensionless conductivity and penetration for a square reservoir - Comparison with the work of Holditch, McGuire & Sikora, and Valko *et al.*

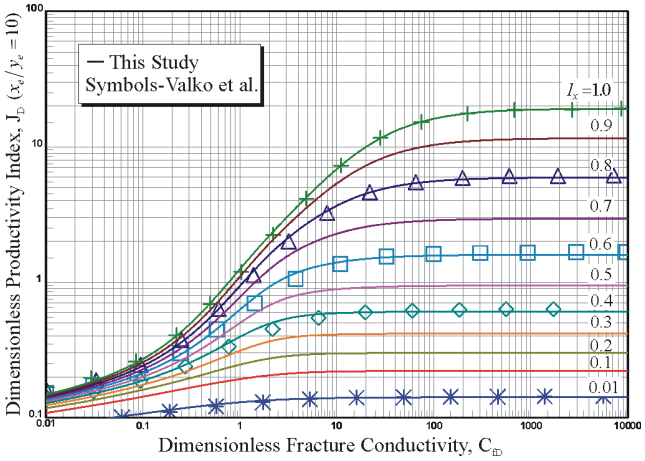

Fig. 30 — Dimensionless productivity index as a function of dimensionless conductivity and penetration for a rectangular reservoir with an aspect ratio of ten - Comparison with the work of Valko and Economides.

As illustrated, this study is in excellent agreement with the numerical results presented by McGuire and Sikora, Holditch, and Valko *et al.* for a square reservoir. Excellent agreement with Valko's numerical results are also shown for the case of a rectangular reservoir with an aspect ratio of ten.

Appendix C: Solutions for Multiple Transverse Fractures in Horizontal Wells

The fundamental production solution methodology for multiple transverse finite-conductivity vertical fractures in horizontal wells is presented. The solution for a single fractured well in a closed system is presented followed by general solutions for Multiply Fractures, Multiple Equally Spaced Transverse Fractures, and Multiple Stage/Cluster Transverse Fractures in horizontal wells.

Single Vertical Fracture

The system configuration for a single finite-conductivity vertical fracture in a closed rectangular reservoir with aspect ratio ($\lambda = x_e/y_e$) is illustrated in Figure 31.

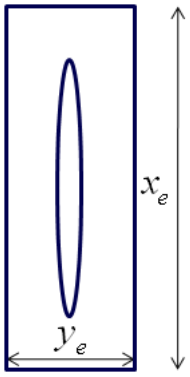

Fig. 31 — Schematic of a single hydraulic fracture in a closed rectangular reservoir - top view.

The fundamental dimensionless solutions are

Constant Rate

$$p_D(t_D, \lambda) = \frac{2\pi kh}{q\mu}\Delta p(t), \text{ where } \Delta p(t) = \frac{q\mu}{2\pi kh}p_D(t_D, \lambda) \tag{C.1}$$

Constant Pressure

$$q_D(t_D, \lambda) = \frac{\mu}{2\pi kh\Delta p}q(t), \text{ where } q(t) = \frac{2\pi kh\Delta p}{\mu}q_D(t_D, \lambda) \tag{C.2}$$

Multiply Fractures

The system configuration for multiple vertical fractures equally spaced in a closed rectangular reservoir with aspect ratio ($\lambda = x_e/y_e$) is shown Figure 32.

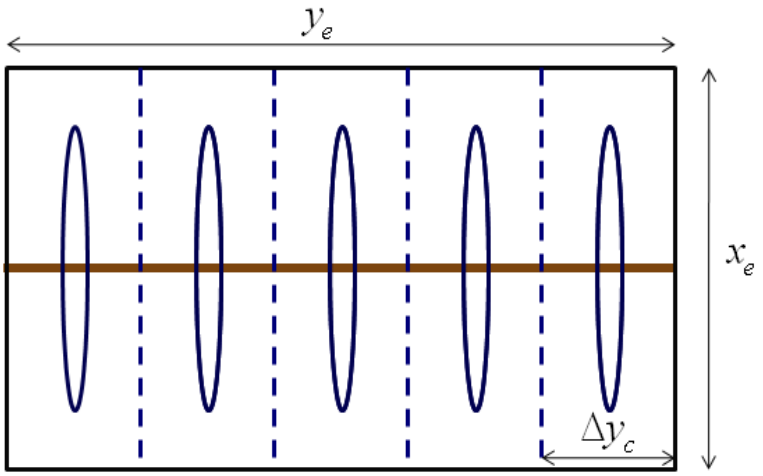

Fig. 32 — Schematic of multiply fractures in a closed rectangular reservoir - top view.

The no flow boundary conditions are identified by dashed lines. The individual fractured reservoir aspect ratio is given by $\lambda_c = x_e/\Delta y_c$ or $\lambda_c = \lambda N$ where $\Delta y_c = y_e/N$, $\lambda = x_e/y_e$, and N is the number of fractures. The total flow rate is found by multiplying the single well fracture solution with an aspect ratio of λ_c by N.

The fundamental dimensionless pressure and rate solutions for N multiple fractures are

Constant Rate

$$p_D = p_D(t_D, \lambda_c)/N \tag{C.3}$$

Constant Pressure

$$q_D = q_D(t_D, \lambda_c) \cdot N \tag{C.4}$$

This solution is referred to as Multiply Fractures since the total rate for a constant draw down pressure is simply the single fracture production solution multiplied by the total number of transverse fractures (see also Guo and Evans (1993)). This is an exact solution methodology.

Multiple Equally Spaced Transverse Fractures - Lateral Length

The system configuration for N equally spaced transverse fractures over a given lateral length in a closed rectangular reservoir with aspect ratio (λ) is shown in Figure 33.

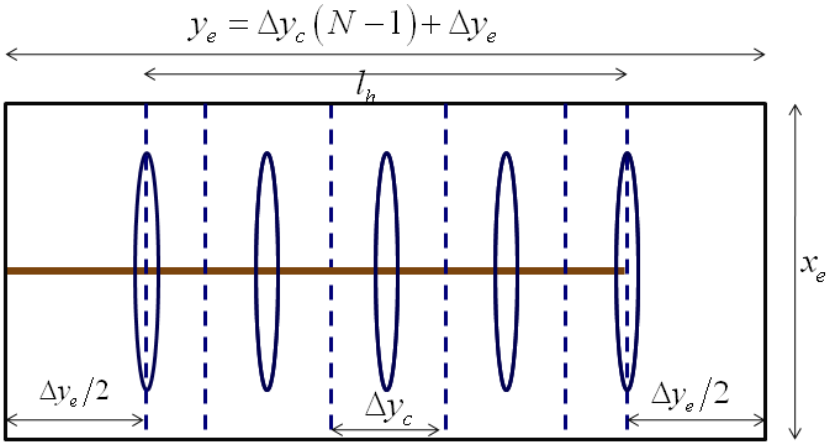

Fig. 33 — Schematic of a multiple transverse fractures in a closed rectangular reservoir - top view.

The no flow boundary conditions are identified by dashed lines. The individual fractured reservoir aspect ratios for the cluster and end fractures are given by

Clusters

$$\lambda_c = x_e/\Delta y_c$$

End or Exterior

$$\lambda_e = x_e/\Delta y_e \tag{C.5}$$

The cluster spacing is found from $\Delta y_c = l_h/(N-1)$. The spacing from the exterior fracture to the boundary is given by $\Delta y_e/2$ where $\Delta y_e = y_e - l_h$.

The fundamental dimensionless pressure and rate solutions for N multiple equally spaced fractures over a given lateral length are

Constant Rate

$$p_D = \frac{p_D(t_D,\lambda_c)\cdot p_D(t_D,\lambda_e)}{p_D(t_D,\lambda_e)(N-1)+p_D(t_D,\lambda_c)} \tag{C.6}$$

Constant Pressure

$$q_D = q_D(t_D,\lambda_c)(N-1)+q_D(t_D,\lambda_e) \tag{C.7}$$

These are not exact solutions but very good first-order approximations. The above equations simplify to the Multiply Fractures solution for equally spaced fractures (i.e., $\lambda_e = \lambda_c$).

Multiple Stage/Cluster Transverse Fractures

The system configuration for multiple stage/clusters with n_s equally spaced stages and n_c equally spaced clusters per stage in a closed rectangular reservoir with aspect ratio (λ) is shown in Figure 34.

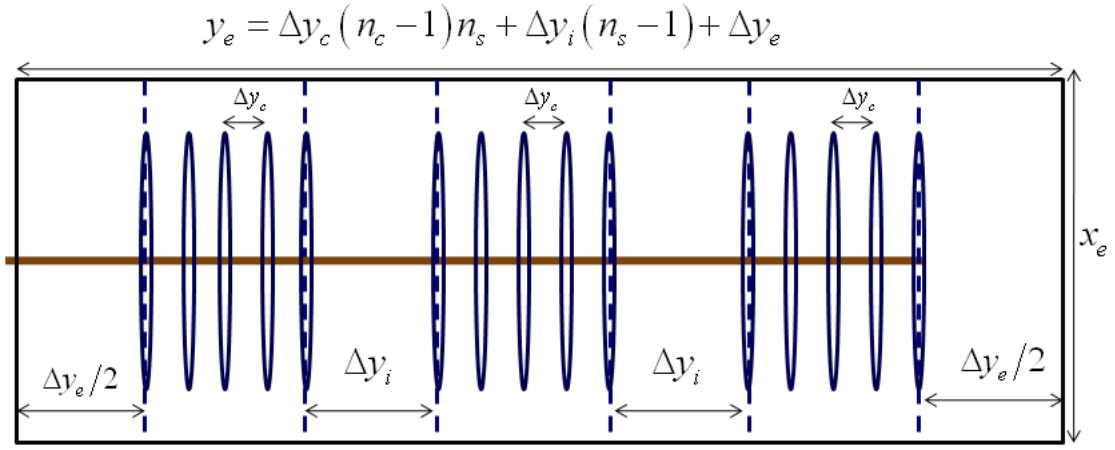

Fig. 34 — Schematic of a multiple stage/cluster transverse fractures in a closed rectangular reservoir - top view.

The no flow boundaries for each cluster set are identified by dashed lines. The reservoir and no flow boundary aspect ratios for the clusters, interior, and exterior transverse fractures are

Clusters

$$\lambda_c = x_e/\Delta y_c$$

Interior

$$\lambda_i = x_e/\Delta y_i \tag{C.8}$$

End or Exterior

$$\lambda_e = x_e/\Delta y_e$$

where the cluster spacing is given by Δy_c, the interior spacing between cluster stages is given by Δy_i, and the spacing from the exterior fracture to the boundary is given by $\Delta y_e/2$. The total number of transverse fractures is $N = n_c \cdot n_s$.

The fundamental dimensionless pressure and rate solutions for multiple stage/cluster transverse fractures are

Constant Rate

$$p_D = \frac{p_D(t_D, \lambda_c) \cdot p_D(t_D, \lambda_i) \cdot p_D(t_D, \lambda_e)}{p_D(t_D, \lambda_i) \cdot p_D(t_D, \lambda_e)(n_c - 1)n_s + p_D(t_D, \lambda_c) \cdot p_D(t_D, \lambda_e)(n_s - 1) + p_D(t_D, \lambda_c) \cdot p_D(t_D, \lambda_i)} \tag{C.9}$$

Constant Pressure

$$q_D = q_D(t_D, \lambda_c)(n_c - 1)n_s + q_D(t_D, \lambda_i)(n_s - 1) + q_D(t_D, \lambda_e) \tag{C.10}$$

These are not exact solutions but very good first-order approximations for various complicated stage/cluster configurations. For equally spaced inner and cluster fractures (i.e., $\lambda_i = \lambda_c$), the above equations simplify to the Multiple Equally Spaced Transverse Fractures solution

Constant Rate

$$p_D = \frac{p_D(t_D, \lambda_c) \cdot p_D(t_D, \lambda_e)}{p_D(t_D, \lambda_e)(n_c - 1)n_s + p_D(t_D, \lambda_e)(n_s - 1) + p_D(t_D, \lambda_c)} = \frac{p_D(t_D, \lambda_c) \cdot p_D(t_D, \lambda_e)}{p_D(t_D, \lambda_e)(n_c n_s - 1) + p_D(t_D, \lambda_c)} \tag{C.11}$$

Constant Pressure

$$q_D = q_D(t_D, \lambda_c)(n_c n_s - 1) + q_D(t_D, \lambda_e) \tag{C.12}$$

where $N = n_c n_s$.

For equally spaced fractures (i.e., $\lambda_e = \lambda_i = \lambda_c$), the above equations simplify to the Multiply Fractures solution as illustrated below

Constant Rate

$$p_D = \frac{p_D(t_D, \lambda_c)}{(n_c - 1)n_s + (n_s - 1) + 1} = \frac{p_D(t_D, \lambda_c)}{n_c n_s} = \frac{p_D(t_D, \lambda_c)}{N} \tag{C.13}$$

Constant Pressure

$$q_D = q_D(t_D, \lambda_c)[(n_c - 1)n_s + (n_s - 1) + 1] = q_D(t_D, \lambda_c)n_c n_s = q_D(t_D, \lambda_c)N \tag{C.14}$$

Appendix D: Transverse Fracture Interference

The interference of multiple transverse fractures is evident by the no flow boundary conditions imposed by the solution methodology as presented in Appendix C.

The subject of well interference is not a new concept. Stevens and Thodos (1959) presented one of the first papers on "Prediction of Approximate Time of Interference Between Adjacent Wells" based on a point-source function. Warren and Hartsock (1960) also published a paper entitled "Well Interference". Other notable contributors to this area of study include Vela and Mckinley (1969), Mousli *et al.* (1982), Cooper and Collins (1989), Meehan *et al.* (1989), and Malekzadeh and Tiab (1991).

A simple solution to understand this concept of fracture interaction or interference was present by Lee *et al.* (1996, 2003). Lee entitled this behavior as the "Radius of Investigation Concept". Lee states, "The radius of investigation, defined as the point in the formation beyond which the pressure draw down is negligible, is a measure of how far a transient has moved into the formation following any rate change in a well and physically represents the depth to which formation properties are being investigated at any time in a test." Lee gives the approximate radius of investigation at any time as

$$r_i = \left(\frac{kt}{948\phi\mu c_t}\right)^{1/2} \tag{D.1}$$

Applying this concept to multiple transverse fractures spaced a distance Δy apart (i.e., $\Delta y = 2r_i$), we have

$$\Delta y = \left(\frac{4kt}{948\phi\mu c_t}\right)^{1/2} = \left(\frac{\eta t}{237}\right)^{1/2} \tag{D.2}$$

where the formation diffusivity, η, is given by $\eta = k/(\phi\mu c_t)$. Average property values should be used for gas.

Thus, the approximate time for transverse fracture interaction (i.e., time to reach the no flow boundary) is

$$t = 237\frac{\Delta y^2}{\eta} \tag{D.3}$$

Figure 35 shows the interference spacing as a function of diffusivity for various selected times. This figure illustrates that as diffusivity increases the time for transverse fracture interference decreases.

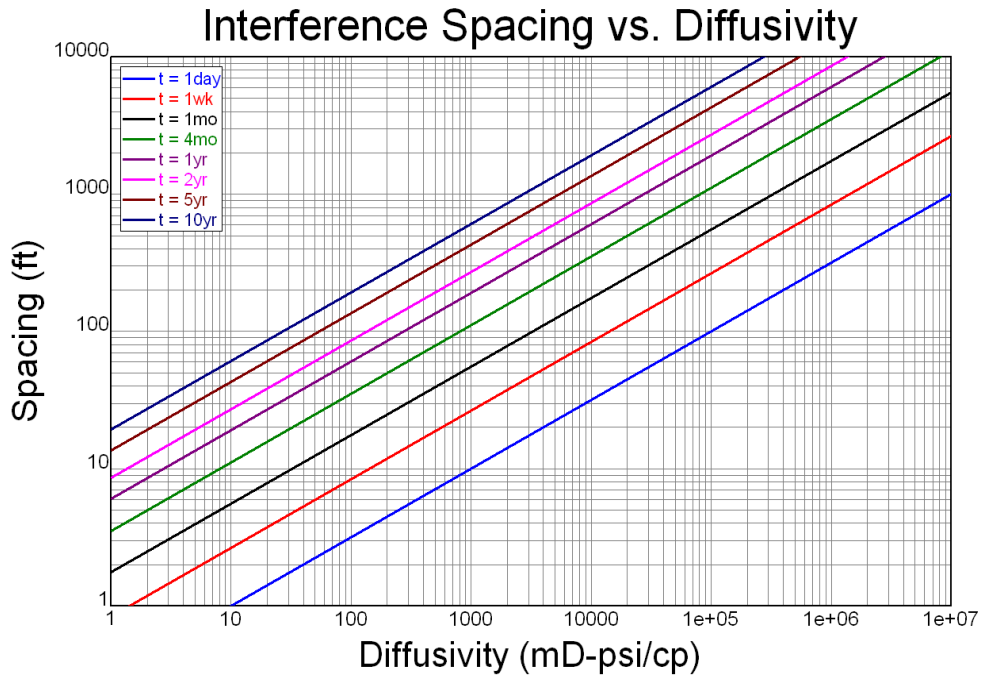

Fig. 35 — Interference distance versus formation diffusivity for various times.

Figure 36 shows the interference spacing as a function of time for selected diffusivities. Figure 36 illustrates that as the formation diffusivity increases, the transverse fracture spacing increases for a given time to interference.

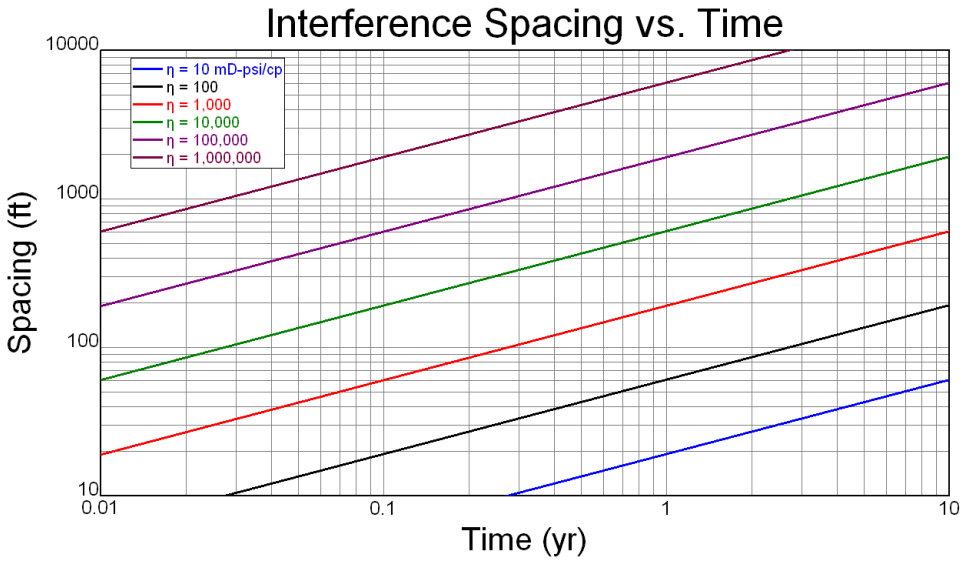

Fig. 36 — Interference spacing versus time for selected diffusivity values.

Appendix E: General Economic Equations

This section presents the equations used for conducting economic optimization.

Fracture Net Present Value (NPV)

The present value or present worth, P, of a future-value, F, is

$$P = \frac{F}{(1+i)^n} \tag{E.1}$$

where

P = present worth
F = future worth
i = currency escalation rate or interest rate
n = number of periods

This formula is the basis for calculating the Net Present Value of an investment. Fracture Net Present Value, NPV, is defined as the revenue from a hydraulically fractured reservoir less the production from the same reservoir without a hydraulic fracture and the cost of the treatment in current dollars. This relationship is expressed as follows

$$NPV = R_F - R_0 - C_F \text{ or } NPV = \sum_{j=1}^{n} \frac{(V_F)_j}{(1+i)^j} - \sum_{j=1}^{n} \frac{(V_0)_j}{(1+i)^j} - C_F \tag{E.2}$$

where

C_F = total fixed and variable cost of a fracture treatment
n = number of periods
NPV = fracture Net Present Value
R_F = present value production revenue of a fractured reservoir
R_0 = future value production revenue of an unfractured reservoir
V_F = future value production revenue of a fractured reservoir
V_0 = future value production revenue of an unfractured reservoir

Discount Well Revenue (DWR)

The Discounted Well Revenue (DWR) in terms of the net incremental cash flow, NCF_j, is

$$DWR = \sum_{j=1}^{n} \frac{(V_F)_j}{(1+i)^j} - \sum_{j=1}^{n} \frac{(V_0)_j}{(1+i)^j} \text{ or } DWR = \sum_{j=1}^{n} \frac{(NCF)_j}{(1+i)^j} \tag{E.3}$$

The NPV can be expressed in terms of the DWR by

$$NPV = DWR - C_F \tag{E.4}$$

From these expressions it is shown that the fracture NPV is a function of time, propped fracture length, conductivity, drainage area, reservoir properties, etc. This methodology, therefore, is an excellent criteria for basing the optimization strategy.

Discounted Return on Investment (DROI)

The DROI also takes into account the time value of money invested and can be used as a indicator of the capital investment efficiency. The DROI is simply the ratio of the Discounted Well Revenue (DWR) divided by the total cost of a treatment, C_F, as given by

$$DROI = (DWR)/C_F \tag{E.5}$$